minerals

Article

# Geochronology and Isotope Geochemistry of the Yingfang Pb-Zn-Ag Deposit: Implications for Large-Scale Metallogeny along the Northern Flank of the North China Craton

**Xiaoyan Liu [1,2], Lin Li [1,3,*], Shengrong Li [1,2], M. Santosh [2,4] and Yujie Li [5]**

1 State Key Laboratory of Geological Processes and Mineral Resources, China University of Geosciences, Beijing 100083, China; liuxiaoyan010624@163.com (X.L.); lisr@cugb.edu.cn (S.L.)
2 School of Earth Science and Resources, China University of Geosciences, Beijing 100083, China; santosh@cugb.edu.cn
3 Institute of Earth Science, China University of Geosciences, Beijing 100083, China
4 Department of Earth Sciences, University of Adelaide, Adelaide, SA 5005, Australia
5 China Mining Association, Beijing 100029, China; linxuanchenmeng@163.com
* Correspondence: clark.li@cugb.edu.cn

**Abstract:** The northern flank of the North China Craton (NCC) hosts a linear zone of gold, molybdenum, silver, lead, and zinc polymetallic ore deposits. Among these, the Yingfang Pb-Zn-Ag deposit is located in the central part of the Yanshan–Liaoxi metallogenic belt (YLMB) which extends for approximately 1000 km and forms part of the major mineralized zone. In this study, we characterize the mineralization and trace the ore genesis based on new sulfur and lead isotopic geochemistry and evaluate the timing of mineralization from Rb-Sr isotope dating of sulfides. The pyrite $\delta^{34}S$ values range from +3.2‰ to +5.8‰ with a mean at +4.07‰, close to the values of mantle and meteorite sulfur. The $^{206}Pb/^{204}Pb$ values range from 16.833 to 18.956, $^{207}Pb/^{204}Pb$ from 15.374 to 15.522, and $^{208}Pb/^{204}Pb$ from 37.448 to 37.928. Five samples of sulfide, from the Yingfang deposit, yield a Rb-Sr isochron age of 135.7 ± 4.1 Ma. This age is close to the age of the adjacent Niujuan Ag-Au deposit and the associated Er'daogou granite, suggesting a close relationship between magmatism and metallogeny in this region. The S and Pb isotopes of the regional silver polymetallic deposits show similar sources of ore-forming materials. According to a compilation of the available age data on the Mesozoic ore deposits in the northern flank of the NCC, we divide the mineralization into the following four periods: 240–205 Ma, 190–160 Ma, 155–135 Ma, and 135–100 Ma. Mesozoic magmatism and mineralization in the Yingfang deposit mainly took place at 245 Ma and 145–135 Ma. We correlate the Pb-Zn-Ag mineralization to metallogeny associated with large-scale inhomogeneous lithosphere thinning beneath the NCC.

**Keywords:** S-Pb isotopes; sulfide Rb-Sr geochronology; Yingfang Pb-Zn-Ag deposit; large-scale metallogeny; northern flank of the North China Craton

check for updates

**Citation:** Liu, X.; Li, L.; Li, S.; Santosh, M.; Li, Y. Geochronology and Isotope Geochemistry of the Yingfang Pb-Zn-Ag Deposit: Implications for Large-Scale Metallogeny along the Northern Flank of the North China Craton. *Minerals* **2021**, *11*, 353. https://doi.org/10.3390/min11040353

Academic Editor: Maria Boni

Received: 23 February 2021
Accepted: 22 March 2021
Published: 29 March 2021



## 1. Introduction

The northern flank of the North China Craton (NCC) hosts several important gold, molybdenum, silver, lead, and zinc polymetallic ore deposits in China (Figure 1a,b) [1–3]. These deposits occur in an east–west trending linear zone that extends for almost 1500 km. Three main metallogenic belts are defined, from west to east, termed the Langshan–Baiyunebo, Yanshan–Liaoxi, and Liaodong-Ji'nan metallogenic belts (Figure 1b) [4–6].

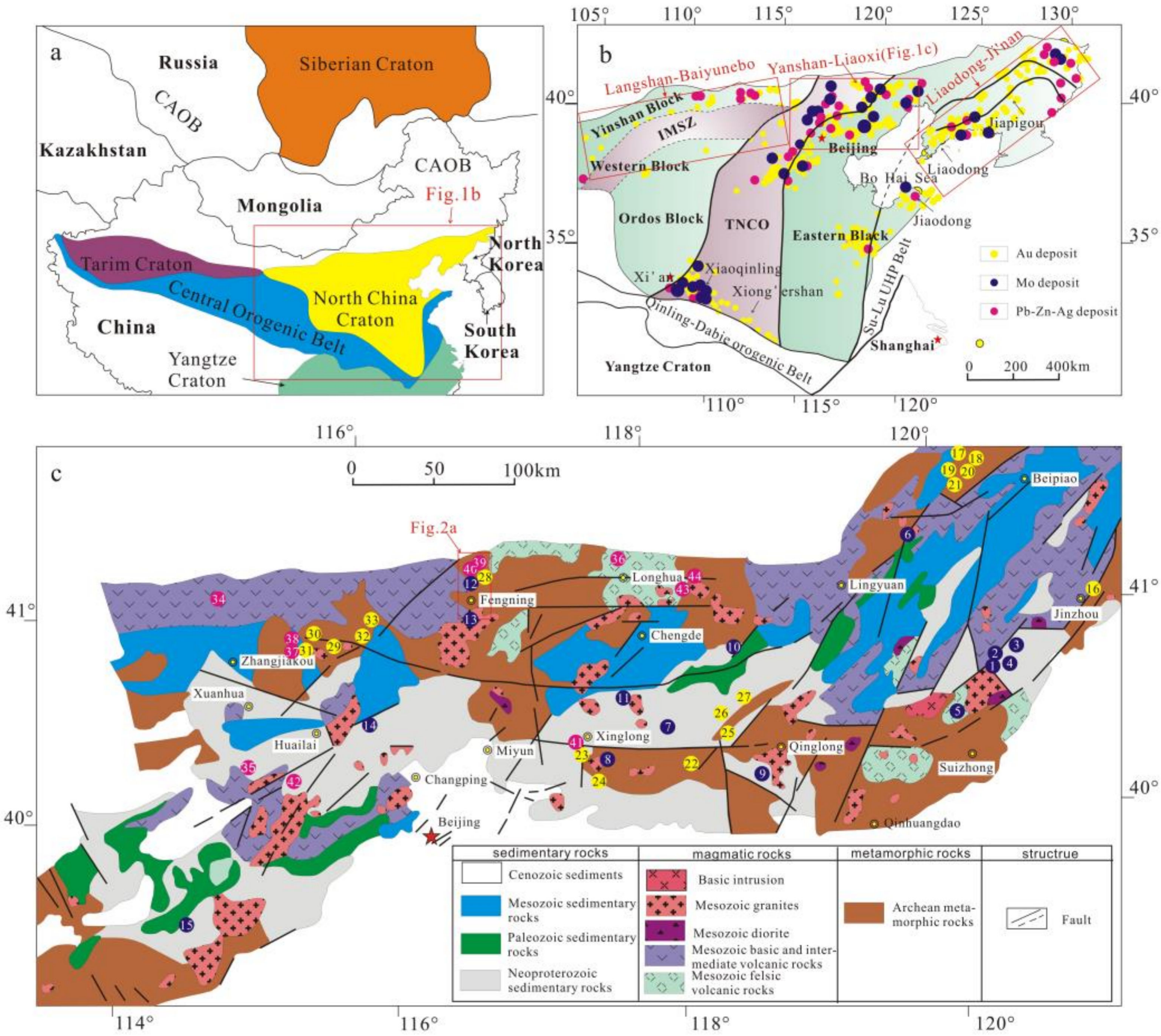


**Figure 1.** (**a**) Simplified tectonic map of China showing the major cratons (after [7]); (**b**) Sketch map of the NCC showing the distribution of silver-polymetallic deposits (after [3,8]). IMSZ, Inner Mongolia Suture Zone; TNCO, Trans-North China Orogen; (**c**) Distribution of the silver and polymetallic deposits in the Yanshan–Liaoxi metallogenic belt (modified from [9]). Data sources and deposit numbers are listed in Table 2.

Several new Au, Mo, Ag, Pb, and Zn polymetallic deposits were recently discovered in the Yanshan–Liaoxi metallogenic belt (YLMB), the central segment along the northern flank of the NCC (Figure 1c) [9–13]. The YLMB comprises a series of porphyry-, skarn-, quartz vein-, altered rock- and epithermal-ore deposits. Located in the central part of the YLMB, the Yingfang Pb-Zn-Ag deposit is spatially associated with Mesozoic intrusions and occurs along the contact between the intrusions and Paleoproterozoic metamorphic rocks (Figure 2a,b). The deposit has an estimated reserve of 1.61 Mt Pb with an average grade of 4.29 wt.%, 1.68 Mt Zn with an average grade of 3.16 wt.%, and 592 t Ag with an average grade of 171 g/t (North China Mineral Exploration Development Bureau 514 Geological Team, Exploration report, 2001, unpublished).

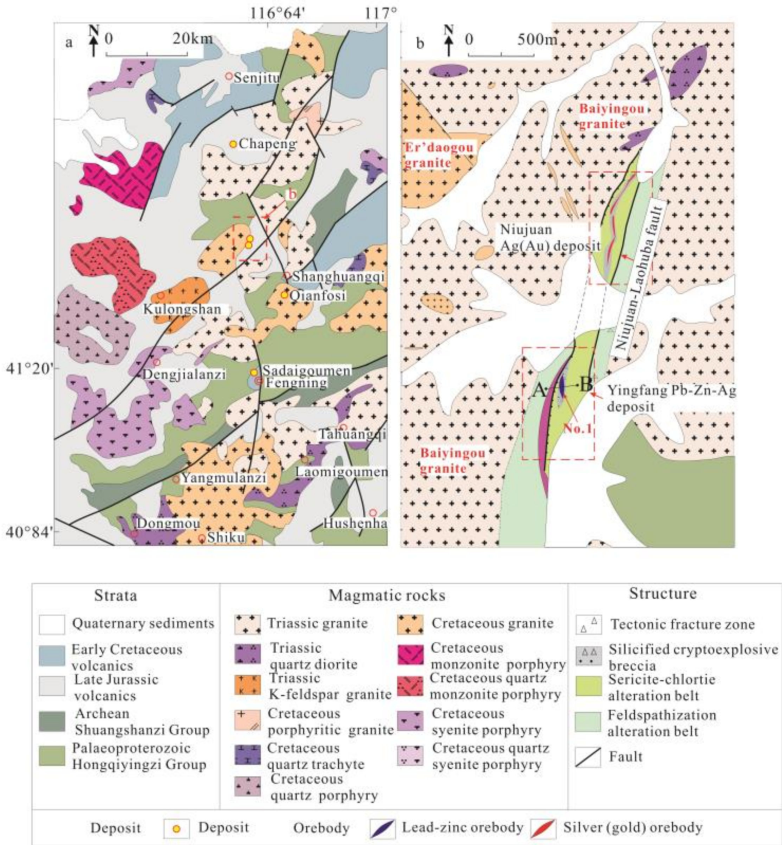


**Figure 2.** (**a**) Regional geological map of the Fengning area showing the distribution of magmatic rocks (modified from [14]); (**b**) Geological map of the Niujuan Ag (Au) deposit and the Yingfang Pb-Zn-Ag deposit (A–B: exploration line; modified after [13,15]).

This region exposes voluminous igneous rocks [16], most of which were emplaced during Jurassic to Early Cretaceous (185–80 Ma), and a minor volume during Paleozoic [11,16,17]. The complex tectonic processes associated with cratonization, the later destruction of the NCC, and the related multiple magmatic activities provided favorable conditions for metallogeny in this region [2,3,18,19]. Previous studies on Ag, Pb, and Zn polymetallic deposits generally have focused on their geological characteristics [10,11,16], ore-controlling factors [1,20], fluid inclusions, associated magmatism [15,21,22], and timing of ore formation [13,23,24]. However, the relationship between magma emplacement and polymetallic mineralization, as well as the corresponding geodynamic settings of Mesozoic magmatism and mineralization in this region, remain debated. The source of ore-forming materials of Au-Ag polymetallic deposits of the YLMB remains controversial both with respect to theoretical models and exploration strategies. A systematic compilation of previous geochemical data is helpful to understand the origin of the deposits in a broad perspective. Although an important deposit in the YLMB, few studies have been carried out on the Yingfang deposit. These studies were focused mainly on dating the intrusions or gangue minerals associated with the Pb-Zn-Ag mineralization to determine the formation age of the Yingfang deposit [2,15]. On the basis of the geological relationship and the zircon U-Pb ages, the Pb-Zn-Ag mineralization was inferred to be later than the emplacement of the Er'daogou fine-grained granite (145 Ma) [2]. The timing of Pb-Zn mineralization has not been constrained. In this study, we used sulfides Rb-Sr methods to date the sulfides in the ores in order to constrain the mineralization time, and we documented stable isotopic data on the ore sulfides in order to gain better insights on the ore-forming materials in the Yingfang deposit. According to our new data and those from previous work, we evaluate the relationship between magmatism and Ag, Pb, and Zn polymetallic mineralization with a view to understanding the link between regional geodynamics and Ag, Pb, and Zn mineralization.

## 2. Geological Setting

The Yanshan–Liaoxi metallogenic belt (YLMB, 39°30′–41°20′ N, 114°00′–120°50′ E) is located in the northern flank of the NCC (Figure 1a), covering the northern Hebei and western Liaoning provinces [6]. The Archean-Paleoproterozoic crystalline basement in this region comprises migmatite, amphibolite-greenschist, and granulite facies rocks. The Neoproterozoic sedimentary cover, up to 10 km in thickness, is related to the intra-cratonic aulacogen rifting processes in this region, consisting of bathyal to shallow sea clastic and carbonate rocks including fine-grained sandstone, shale, dolomite, and limestone. The Phanerozoic strata can be divided into four sequences as follows: (1) Cambrian-Middle Ordovician shallow-marine carbonates, composed of limestone, dolomitic limestone, muddy limestone, oolitic limestone, and shale. (2) Upper Carboniferous-Lower Permian carbonates and coal seam-bearing clastic rocks, consisting of limestone, muddy limestone, dolomitic limestone, limestone, and breccia. (3) Upper Permian-Triassic red beds and conglomerates, represented by limestone, shale, sandstone, and coal beds. (4) Jurassic-Cretaceous continental volcano-sedimentary units, comprising intermediate-basic volcanic lava, felsic volcanic lava, tuff, sandstone, conglomerate, and coal beds [9,16,25]. In addition to volcano-sedimentary rocks, the Mesozoic plutonic rocks are also widely distributed in the YLMB, including granitoids, diorite, syenite porphyrite, lamprophyre, gabbro, and dolerite [26,27]. From Early Jurassic to Late Cretaceous, the mafic magmatism evolved into more felsic composition [9]. Most granitoid plutons occur mainly as stocks or dykes, with outcrops covering more than 10 km$^2$ [16,26,28,29]. Fault structures are well developed in the YLMB, showing mainly EW-, NE- and NNE-trends (Figure 1c).

In Mesozoic, the northern margin of the North China experienced the "Yanshan Movement" [30,31] that resulted in uplift and erosion, volcanic eruptions, and magmatic intrusion, as well as large-scale fold, nappe thrust structures. Zhao et al. (2004) [32] proposed the following three tectonic episodes in the YLMB in the Yanshanian: (1) Episode A (175–160 Ma) marked by angular unconformity below the andesites of the Tiaojishan (or Lanqi) Formation volcanic rocks; (2) The intermediate Episode (165–156 Ma) represented by intensive volcanic activity (e.g., the Tiaojishan and Lanqi Formations); (3) Episode B (156–139 Ma) marked by strong fold and nappe thrust structures. From the Early Cretaceous, the tectonic deformation was dominated by extension, with successive volcanic eruptions and associated weak tectonic deformation.

## 3. Orefield Geology

The Yingfang Pb-Zn-Ag deposit is located in the contact region of the Baiyingou granite and the Paleoproterozoic Hongqiyingzi Group metamorphic rocks, and about 0.5 km south of the Niujuan silver deposit. The basement rocks exposed in the southern of Fengning orefield is mainly the Paleoproterozoic Hongqiyingzi Group metamorphic rocks, which comprise biotite plagioclase gneiss and biotite-bearing plagioclase amphibolite. The Baiyingou coarse-grained granite in this orefield occupies most part of the exposed Mesozoic granitoids and is the largest outcrop in this area. The Er'daogou fine-grained granite is distributed in both eastern part and western part of the orefield and is not far from the orebodies. Some felsic dykes, mainly quartz diorite and quartz veins, are also distributed in the region (Figure 2a). The Kangbao-Weichang EW-trending deep fault, Fengning-Longhua NE-trending deep fault, and Shanghuangqi-Wulonggou NNE-trending deep fault are located in the north, west, and east of the Fengning area, respectively. The Niuquan-Laohuba fault ($F_1$), a secondary structure produced parallel to the Shanghuangqi-Wulonggou deep fault, is the main fault in the Fengning area to control rocks and ores and has a close spatial relationship with the Yingfang Pb-Zn-Ag deposit.

Four orebodies are hosted in the Baiyingou coarse-grained granite in the Yingfang Pb-Zn-Ag deposit and are mostly controlled by NNE-trending faults. Among these orebodies, the largest one (No. 1, Figure 2b) is about 425 m in length, 263 m in depth, and around 5.41 m in width, with average grades of 124 g/t Ag, 6.5% Pb, and 3.5% Zn.

The ore minerals are mainly galena, sphalerite, pyrite, chalcopyrite, pyrrhotite, arsenopyrite, and magnetite (Figure 3). The main silver-bearing minerals are argentite, native silver, and freibergite. The main gangue minerals are quartz, calcite, muscovite, biotite, chlorite, and garnet. In addition, sericite, fluorite, and ankerite are also identified in the Yingfang deposit. The ores show xenomorphic granular, euhedral–subhedral granular, exsolution, poikilitic, and intergrowth textures (Figure 3a–f). The xenomorphic granular galena and sphalerite are replaced by the later formed chalcopyrite (Figure 3a). The sphalerite metasomatized galena and the pyroxene distributed in galena along the fracture (Figure 3b). The euhedral–subhedral pyrite and sphalerite grains are intergrown, and chalcopyrite occurs as exsolved blebs in sphalerite crystals (Figure 3c). Pyroxene metasomatism sphalerite, metasomatism edge formed in sphalerite, galena metasomatism natural silver (Figure 3d). Pyrite is cataclastic due to dynamic metamorphism (Figure 3e). The cut surface of pyrite is striped, and pyrite is interbedded with pyrite (Figure 3f).

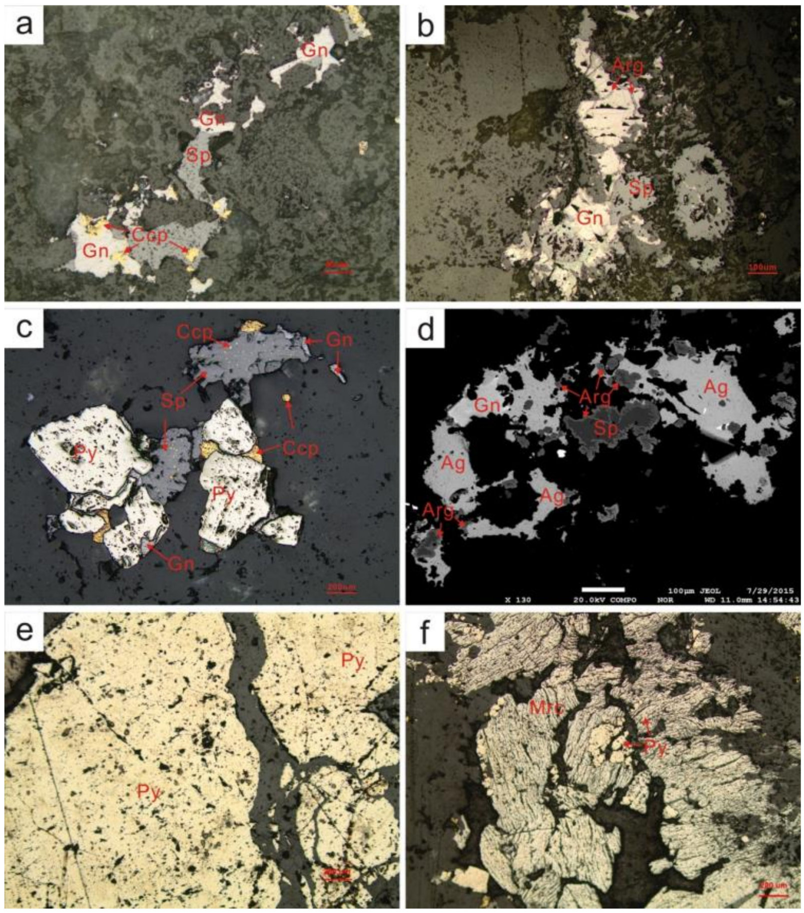


**Figure 3.** Representative photos of ores from the Yingfang deposit (reflected light, d, is backscattered image). (**a**) The chalcopyrite is contained in the late galena sphalerite, which metasomatized the sphalerite (200:1); (**b**) The sphalerite metasomatized galena and the pyroxene distributed in galena along the fracture (100:1); (**c**) Galena and sphalerite metasomatized the earliest pyrite, chalcopyrite dissolved in sphalerite (50:1); (**d**) Pyroxene metasomatism sphalerite, metasomatism edge formed in sphalerite, galena metasomatism natural silver (100:1); (**e**) Pyrite is cataclastic due to dynamic metamorphism (50:1); (**f**) The cut surface of marcasite is striped, and marcasite is interbedded with pyrite (50:1). Ccp, chalcopyrite; Gn, galena; Py-pyrite; Sp, sphalerite; Arg, argentite; Mrc, marcasite.

Hydrothermal alteration in the Yingfang Pb-Zn-Ag deposit consists of silicification, sericitization, kaolinization, chloritization, and carbonatization, with a variety of alteration minerals such as sericite, kaolinite, chlorite, and calcite. Silicification and sericitization are the predominant alteration and show a close relationship with Pb-Zn-Ag mineralization in the Yingfang deposit. Silicic and sericitic alteration are usually overprinted by argillic alteration characterized by the formation of chlorite and kaolinite.

According to the characteristics of the mineral paragenesis, vein crosscutting and the symbiotic relationship among minerals (Figure 4), the dominant ore-forming process in the Yingfang deposit can be divided into the following three stages: early mineralization stage (Stage I), main mineralization stage (Stage II), and late mineralization stage (Stage III). The mineral paragenetic sequences of the three stages in the Yingfang deposit are shown in Figure 5. The three stages are characterized as follows:

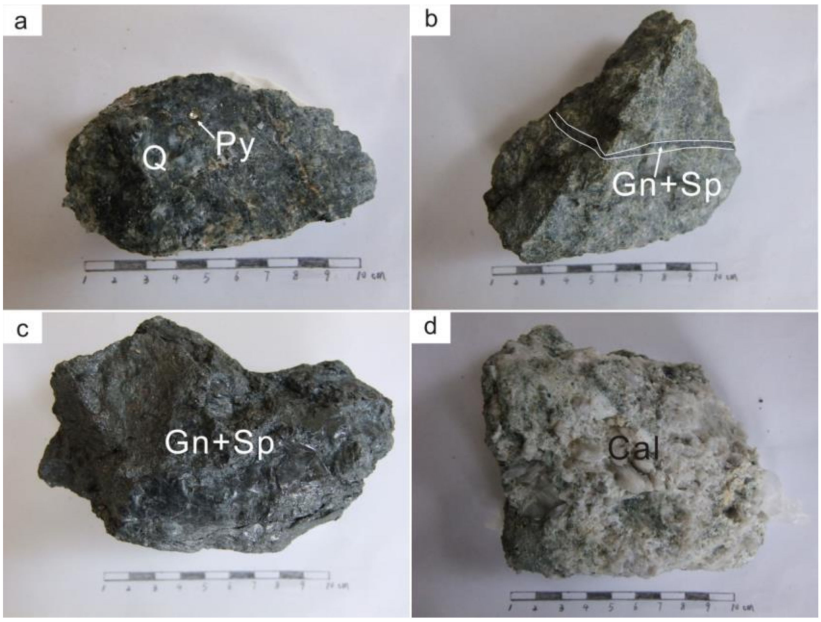


**Figure 4.** Representative specimens of different metallogenic stages of Yingfang lead-zinc deposit. (**a**) Automorphic pyrite and quartz of Stage I; (**b**) Sphalerite and galena veins cut through the early siliceous rocks of mineralization of Stage II; (**c**) A massive ore of sphalerite and galena of Stages II; (**d**) Carbonate of Stage III.

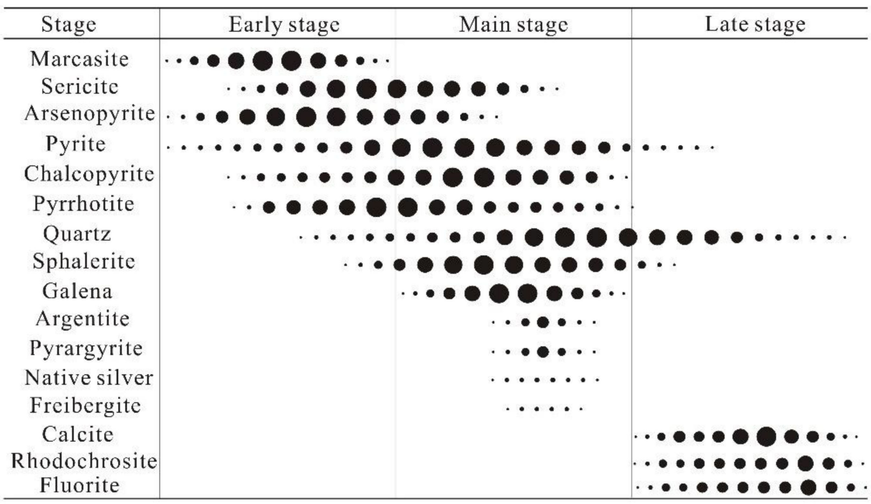


**Figure 5.** Stages of mineralization and the paragenetic sequence of minerals in the Yingfang deposit.

**Early mineralization stage (Stage I)** The main minerals are quartz, sericite, pyrite, arsenopyrite, galena, sphalerite, etc. Pyrite has a coarse particle size, a high degree of idiomorphism, and is distributed in the disseminated form (Figure 4a).
**Main mineralization stage (Stage II)** Characterized by the occurrence of abundant sulfides, such as galena, phalerite, pyrite, chalcopyrite, argentite. The sulfides are often veined in cracks (Figure 4b,c).
**Late mineralization stage (Stage III)** The main minerals are quartz, calcite, and fluorite, etc, and a small amount of rhodochrosite (Figure 4d).

## 4. Sampling and Analytical Methods

### *4.1. Sampling*

The Stage II sulfide samples used for Rb-Sr dating and S-Pb isotopic analyses in this study were collected from the underground mine at a depth of 1090 m in the Yingfang Pb-Zn-Ag deposit. The sulfide minerals occur mainly as disseminations or veinlet minerals in disseminated or massive ores (Figure 4) as follows: (1) Samples 9-45-3(s) and 9-45-3(g) are disseminated Pb-Zn-Ag ores with abundant pyrite; (2) Samples 9-45-2(s) and 9-45-2(g) are massive Pb-Zn-Ag ores with pyrite; and (3) Samples 9-46-1, 9-45-5, and 9-46-5 are massive Pb-Zn-Ag ores.

Sampling was undertaken according the following criteria: (1) to minimize the effect of weathering, (2) to ensure that materials were available from both hanging wall and footwall of Niujuan-Laohuba fault (Figure 2b), and (3) to include representative samples of all the ore types. After crushing and sieving of the representative samples, the separated mineral grains of 40–60 mesh size were handpicked under a binocular stereo microscope to ensure >99% purity.

### *4.2. Analytical Methods*

#### 4.2.1. Rubidium-Strontium Isotopes

The Rb and Sr isotope analyses were carried out using a VG-354 ionization mass spectrometer at the Modern Analysis Center, Nanjing University. The chemical separation and mass spectrometric procedures followed those in [33]. In this study, the measurement of the American Standard Reference Material NBS987 Sr gives $^{87}Sr/^{86}Sr$ value of $0.710233 \pm 0.000006$ (2σ). $^{87}Sr/^{86}Sr$ is normalized to $^{86}Sr/^{88}Sr$ of 0.1194 to correct for instrumental fractionation.

#### 4.2.2. Sulfur and Lead Isotopic Analyses

Sulfur isotopes were determined using a Finnigan MAT-251 mass spectrometer, at the Beijing Research Institute of Uranium Geology, following the procedures outlined by [34]. The precision for $\delta^{34}S$ is better than ±0.2‰ and the data are reported relative to Vienna Canon Diablo Troilite (V-CDT) sulfide. Pb isotopic ratios were analyzed using the same mass spectrometer with an analytical precision better than ±0.2‰.

## 5. Analytical Results

### *5.1. Rb-Sr Isochron Age*

The Rb and Sr isotopic data of Stage II sulfides are listed in Table 1. The Rb contents of the samples are relatively low, ranging from 0.1269 to 0.3927 ppm and the Sr contents are also relatively low, ranging from 0.2256 to 1.698 ppm. The $^{87}Rb/^{86}Sr$ ratios vary from 0.2374 to 5.137 and the $^{87}Sr/^{86}Sr$ ratios from 0.711364 to 0.720768. Regression and age calculations of isochrons were performed using Isoplot/Ex Version 3.00 software (Berkeley Geochronology Center, Berkeley, CA, USA, [35]), and with $\lambda = 1.42 \times 10^{-11}$, using 1% errors for $^{87}Rb/^{86}Sr$ ratios and 0.005% errors for $^{87}Sr/^{86}Sr$ ratios at a confidence level of 95%. The sulfides yield a Rb-Sr isochron age of 135.7 ± 4.1 Ma (MSWD = 2) with an initial $^{87}Sr/^{86}Sr$ ratio of 0.71086 ± 0.00014 (Figure 6).

**Table 1.** Rb-Sr isotopic analyses of sulfides from the Yingfang Pb-Zn-Ag deposit.

| Sample No. | Mineral | Rb(ug/g) | Sr(ug/g) | $^{87}Rb/^{86}Sr$ | $^{87}Sr/^{86}Sr$ | 2σ * | $(^{87}Sr/^{86}Sr)_i$ |
|---|---|---|---|---|---|---|---|
| 9-46-5 | galena | 0.1269 | 1.564 | 0.2374 | 0.711364 | 10 | 0.71091 |
| 9-45-5 | galena | 0.2085 | 1.698 | 0.3621 | 0.711491 | 9 | 0.71080 |
| 9-46-1 | galena | 0.2513 | 1.085 | 0.6802 | 0.712246 | 8 | 0.71094 |
| 9-45-2 | galena | 0.2936 | 0.9142 | 0.9458 | 0.712615 | 11 | 0.71080 |
| 9-45-2 | sphalerite | 0.3927 | 0.2256 | 5.137 | 0.720768 | 9 | 0.71091 |

* **2σ** refers to the error in numerical calculation.

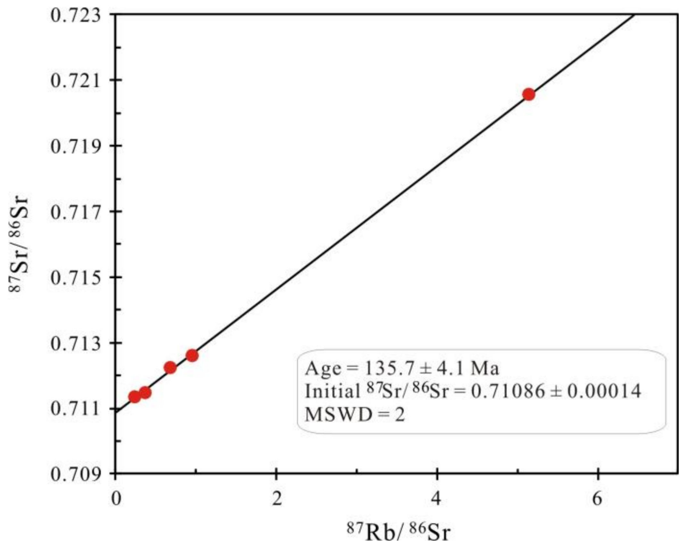


**Figure 6.** Rb-Sr isochron diagram of sulfides from the Yingfang deposit.

### *5.2. S and Pb Isotope Systematics*

Sulfur isotope analyses are listed in Table 2. The $\delta^{34}S$ values of 27 samples (seven samples from this study and the rest compiled from previous studies) range from 3.2‰ to 5.8‰ with a mean value of 4.07‰. The narrow range of $\delta^{34}S$ values suggests that the sulfur in the Yingfang deposit was derived from a common source.

**Table 2.** Sulfur and lead isotope compositions of sulfides from the Yingfang Pb-Zn-Ag deposit.

| Sample No. | Stage | Mineral | $\delta^{34}S_{V\text{-}CDT}$ (‰) * | $\delta^{34}S_{H2S}$ (‰) | $^{206}Pb/^{204}Pb$ | $^{207}Pb/^{204}Pb$ | $^{208}Pb/^{204}Pb$ | $\mu^1$ | $\omega^2$ |
|---|---|---|---|---|---|---|---|---|---|
| 9-45-3(g) | Stage II | Galena | 3.3 | 2.9 | 16.956 | 15.461 | 37.722 | 9.41 | 41.07 |
| 9-45-3(s) | Stage II | Sphalerite | 5.7 | 8.2 | 16.875 | 15.477 | 37.778 | 9.47 | 42.14 |
| 9-46-5(g) | Stage II | Galena | 3.7 | 3.3 | 16.886 | 15.468 | 37.747 | 9.44 | 41.8 |
| 9-45-5(g) | Stage II | Galena | 3.9 | 3.5 | 16.885 | 15.475 | 37.771 | 9.46 | 42.01 |
| 9-46-1(g) | Stage II | Galena | 3.4 | 3.0 | 16.934 | 15.522 | 37.928 | 9.55 | 42.95 |
| 9-45-2(g) | Stage II | Galena | 3.3 | 2.9 | 16.833 | 15.374 | 37.448 | 9.25 | 39.66 |
| 9-45-2(s) | Stage II | Sphalerite | 5.8 | 8.3 | 16.863 | 15.422 | 37.604 | 9.35 | 40.74 |

* $\delta^{34}S_{V\text{-}CDT}$ (‰): Sulfur isotope compositions of sulfides; CDT: Chondrite; $^1\mu = ^{238}Pb/^{204}Pb$; $^2\omega = ^{232}Th/^{204}Pb$.

Lead isotope data from the Yingfang deposit are listed in Table 2. The results show $^{206}Pb/^{204}Pb$ values of 16.833–16.956 (average at 16.89), $^{207}Pb/^{204}Pb$ values of 15.374–15.522 (average at 15.457), and $^{208}Pb/^{204}Pb$ values of 37.448–37.928 (average at 37.714).

## 6. Discussion

### *6.1. Timing of Ore Mineralization*

The precise dating of mineralization has important implications for understanding the duration of ore-forming systems and their temporal relationship to various geological events. Shepherd and Darbyshire (1981) [36] first demonstrated the feasibility of obtaining Rb-Sr fluid inclusion isochrons by analyzing the Rb and Sr isotopic compositions in inclusions within quartz from a tungsten vein-type deposit, which confirmed the significance of fluid inclusions as precise Rb–Sr geochronometers. In recent years, important breakthroughs have been made in constraining the timing of mineralization by the Rb-Sr isochron ages of ore minerals or gangue minerals related to mineralization [37–45]. To get precise Rb-Sr isochron date, all samples are expected to be homologous and formed in the same stage, and the isotopic systems should be closed [46]. Most of the samples in this study are collected from the main mineralization stage (Stage II) and are well crystallized without any fractures, and therefore the Rb-Sr isochron age, in this study (135.7 ± 4.1 Ma), can be used to constrain the mineralization age of the Yingfang deposit.

### *6.2. Origin of the Ore-Forming Constituents*

The stable isotopic composition of sulfide minerals is a useful tool to constrain the origin of hydrothermal fluids [47]. Sulfur isotopic composition of the hydrothermal system is determined by the following physicochemical conditions: (1) isotopic composition of the hydrothermal fluid from which the mineral was deposited, (2) temperature of deposition, (3) chemical composition of the dissolved element species including pH and $f(O_2)$ during mineralization, and (4) relative amount of the minerals deposited from fluids [48–50]. Sulfur isotopic composition of hydrothermal sulfides depends not only on the $\delta^{34}S$ value of source materials, but also on the physicochemical condition of the ore-forming fluid [51]. Therefore, determining the total S isotopic composition ($\delta\Sigma S$) of the hydrothermal fluids during sulfide precipitation is essential for tracing the sulfur source. However, under equilibrium hydrothermal conditions where $H_2S$ is the dominant sulfur species in the fluid, the average $\delta^{34}S$ ($H_2S$) values will approximate the $\delta\Sigma S$ value of hydrothermal fluid [49,52].

In the Yingfang Pb-Zn-Ag deposit, the dominant S-bearing minerals formed during Stage II are all sulfides, including galena, sphalerite, and pyrite, which indicate a relatively simple paragenesis. The $\delta^{34}S$ values obtained from the three sulfides show a general evolution of $\delta^{34}S_{pyrite} > \delta^{34}S_{sphalerite} > \delta^{34}S_{galena}$ (Table 2), suggesting the equilibrium fractionation of sulfur isotope among these sulfide minerals and the ore-forming fluid [53,54]. The $\delta^{34}S$ ($H_2S$) values, therefore, can directly represent the $\delta^{34}S$ value of total sulfur ($\delta\Sigma^{34}S$) of the fluids. According to the study of [55], the $\delta^{34}S(H_2S)$ values involved in hydrothermal system can be calculated as follows:

$$\delta^{34}S_{H2S} = \delta^{34}S_i - A_i \times (10^6 \times T^{-2}) \tag{1}$$

where $i$ refers to different sulfides; A$i$ value is 0.4 for pyrite, 0.1 for sphalerite, and −0.63 for galena, respectively; $T$ (in degrees kelvin) refers to the equilibrium temperature at which the sulfide minerals are deposited. It is calculated by the following formula [56]: $\triangle^{34}\delta_{Sp\text{-}Gn} = \delta^{34}S_{Sp} - \delta^{34}S_{Gn} = 1000\ln a_{Sp\text{-}Gn} = 0.87 \times 10^6 t^{-2} - 0.57$, where "$t$" is the temperature in degrees celsius ($T = t + 273.15$). Mineral twin samples 9-45-3(g), 9-45-3(s) and 9-45-2(g), 9-45-2(s) (Table 2) were adopted for the calculation of the equilibrium temperature. The equilibrium temperature values range from 267 °C to approximately 278 °C, with an average of 272.5 °C for Equation (1).

The $\delta^{34}S(H_2S)$ values range from 2.8‰ to 8.3‰ (Table 2) and are close to those of meteorite and mantle, suggesting a homogeneous source with the involvement of mantle-derived components during the ore-forming processes [51,57]. The $\delta^{34}S$ values of samples from the Mesozoic intrusions (Er'daogou fine-grained granite and Baiyingou coarse-grained granite) that formed during the main magmatic activity are from −0.5‰ to

7.7‰ [13], suggesting a genetic relationship between the ore-forming fluid of the Yingfang Pb-Zn-Ag deposit and the Mesozoic intrusions (Figure 7).

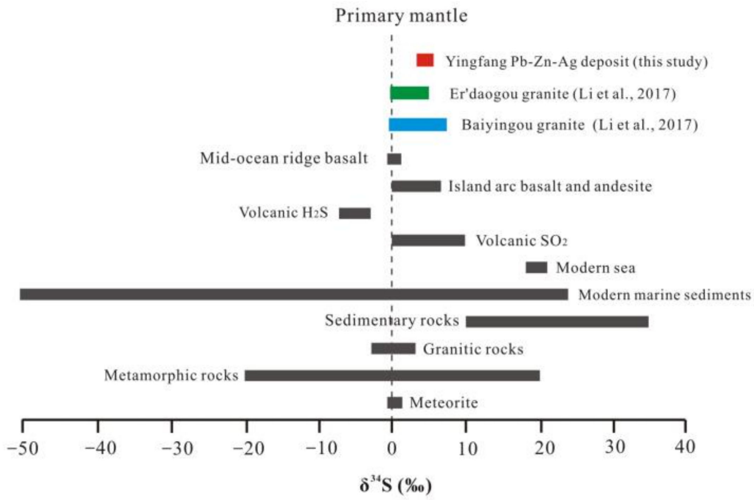


**Figure 7.** Sulfur isotopic composition of sulfides and granites from the Yingfang deposit (after [2]).

Single-stage lead model ages (*t*)were calculated with the equation as follows:

$$[(^{207}\mathrm{Pb}/^{204}\mathrm{Pb} - \mathrm{b}_0)/(^{206}\mathrm{Pb}/^{204}\mathrm{Pb} - \mathrm{a}_0)] = [(\mathrm{e}^{\lambda 5\mathrm{Y}} - \mathrm{e}^{\lambda 5t})/(\mathrm{e}^{\lambda 8\mathrm{Y}} - \mathrm{e}^{\lambda 8t})]/137.88 \quad (2)$$

where Y is the age of the earth; $a_0$ and $b_0$ are the initial lead isotopic compositions of the earth; λ8 and λ5 are the decay constants of $^{238}$U and $^{235}$U, respectively [58].

The single-stage lead model ages obtained range from 1038 to 1119 Ma, which are significantly younger than the ages of the Hongqiyingzi Group metamorphic rocks (2.6–1.7 Ga) [59] but older than the emplacement ages of the Baiyingou coarse-grained granite (245 Ma) [10] and the Er'daogou fine-grained granite (145 Ma) [13] and the mineralization age of the Yingfang Pb-Zn-Ag deposit (135 Ma) (this study). In addition, the lead isotopic values do not plot along the growth curve of single-stage lead in the diagram of $^{207}$Pb/$^{204}$Pb versus $^{206}$Pb/$^{204}$Pb, and the μ and ω values of ore lead (9.25–9.55 and 39.44–42.95, respectively) are obviously higher than the values of normal lead (8.686–9.238 and 35.55 ± 0.59) [58]. On the basis of the above features, it is obvious that the ore lead of the Yingfang Pb-Zn-Ag deposit is radiogenic with complex evolution rather than single-stage normal lead.

The lead isotopic values of sulfides are distributed along a straight line with good linear relation in the diagram of $^{207}$Pb/$^{204}$Pb versus $^{206}$Pb/$^{204}$Pb (Figure 8a). The reference line regressed through the data has a slope of 0.1359 which corresponds to an unrealistic secondary Pb-Pb isochron model age of 2175 Ma [60]. It appears that lead was mobilized from a dominantly single Pb source during discrete hydrothermal events in the Paleoproterozoic. This suggest that the radiogenic ore lead signature might have been contributed by the isotopically evolved Paleoproterozoic basement.

The Pb isotopic compositions of the sulfides from the Yingfang Pb-Zn-Ag deposit show a restricted range in the lead isotope evolution diagrams [61]. As shown in the plot of $^{207}$Pb/$^{204}$Pb versus $^{206}$Pb/$^{204}$Pb (Figure 8a), the Pb isotopic data for sulfides plot in the region between the curves of orogenic belt and mantle evolution. However, in the $^{208}$Pb/$^{204}$Pb versus $^{206}$Pb/$^{204}$Pb diagram (Figure 8b), the sulfide data show a linear trend near the lower crust evolution curve. The $\mu$ values of metal sulfides from the Yingfang deposit are between 9.35 and 9.58, which are obviously higher than the mantle value (8.92) and slightly lower than crustal value (9.58) [62], implying that Pb was mainly derived from the crust with a mantle contribution.

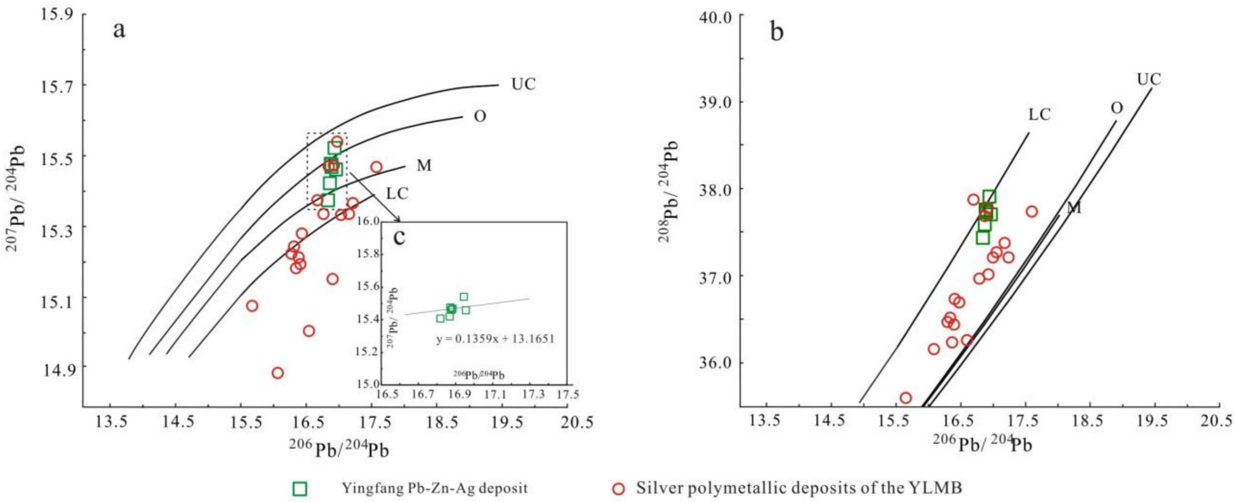


**Figure 8.** Lead isotopic composition of sulfides from the Yingfang deposit and other deposits on the Yanshan–Liaoxi metallogenic belt (YLMB). (**a**) Lead isotope discriminate diagram of $^{207}Pb/^{204}Pb$ versus $^{206}Pb/^{204}Pb$ from [61]; (**b**) Lead isotope discriminate diagram of $^{208}Pb/^{204}Pb$ versus $^{206}Pb/^{204}Pb$ diagram from [61]. (**c**) Lead isotope discriminate diagram of $^{207}Pb/^{204}Pb$ versus $^{206}Pb/^{204}Pb$ from [58]. O, orogen; M, mantle; UC, upper crust contributed to the orogen; LC, lower crust contributed to the orogen. Dotted curves show the lead evolutions fit the data. Data sources and deposit numbers are listed in Table 1.

The $^{87}Sr/^{86}Sr$ ratios are popularly used to trace the source of materials and any crust or mantle contamination of magmatic and deep fluids [40,63]. The $^{87}Sr/^{86}Sr$ values in the Yingfang Pb-Zn-Ag deposit are between 0.71080 and 0.71094, with an average of 0.71087 (Table 1), which are lower than the continental crust average $^{87}Sr/^{86}Sr$ ratio of 0.719 [64] and higher than the mantle initial value of 0.704 [58], indicating that the Sr originated from lower crust with limited input of mantle materials.

### *6.3. Comparison with Other Deposits in the YLMB along the Northern Flank of the North China Craton (NCC)*

Sulfur isotopic data on 332 samples from 20 silver polymetallic deposits in the YLMB show that the Mesozoic ore deposits have values from −14.40‰ to +11.80‰ (Figure 9a and Table 3), with most of the values clustering between 0‰ and 6‰ (Figure 9b). The sulfur isotope compositions of the sulfide minerals from most of these deposits show the characteristics of equilibrium fractionation [2,65,66]. As illustrated in Figure 8a, the sulfur isotope characteristics of the Yingfang deposit are similar to those of other silver polymetallic deposits in the YLMB and are close to meteorite and mantle.

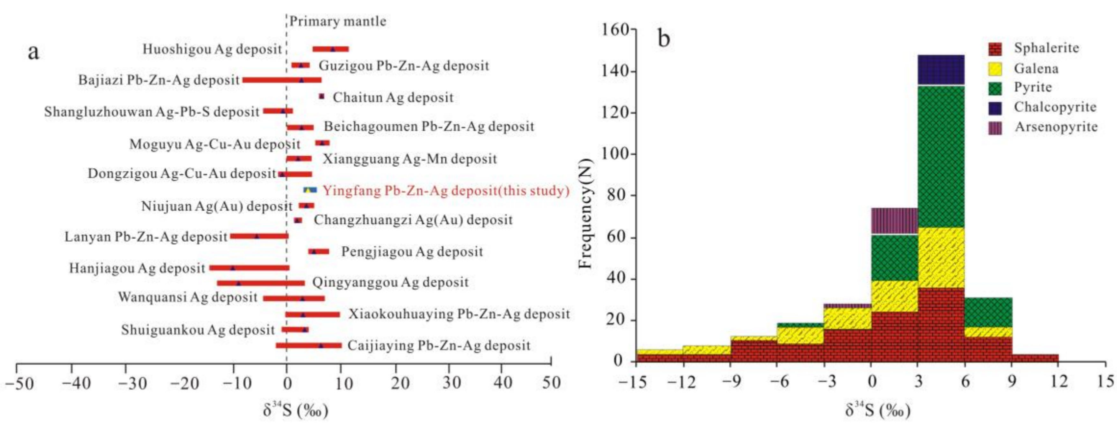


**Figure 9.** Sulfur isotopic composition. (**a**) (Refer to Table 3 for data) and histogram; (**b**) Sulfur isotopic composition of sulfides from the silver polymetallic deposits on the YLMB.

**Table 3.** Sulfur and lead isotope compositions of the silver-polymetallic deposits in the YLMB.

| Deposit | Species | $\delta^{34}S$ (‰) | | Pb | | | Reference |
|---|---|---|---|---|---|---|---|
| | | Range | Mean | $^{206}Pb/^{204}Pb$ | $^{207}Pb/^{204}Pb$ | $^{208}Pb/^{204}Pb$ | |
| Yingfang | Pb-Zn-Ag | 3.2 to 5.8 | +4.07 | 16.89 | 15.46 | 37.71 | This paper |
| Caijiaying | Ag-Pb-Zn | −1.90 to 10.50 | +6.70 | 16.84 | 15.47 | 37.72 | [16] |
| Shuiguankou | Ag | −0.83 to 4.26 | +3.50 | 16.31 | 15.25 | 36.51 | [67] |
| Xiaokouhuaying | Ag-Pb-Zn | −0.13 to 10.14 | 3.20 | 17.15 | 15.34 | 37.39 | [67] |
| Wanquansi | Ag | −4.30 to 7.30 | +3.13 | 16.45 | 15.29 | 36.69 | [67] |
| Qingyanggou | Ag | −12.96 to 3.54 | −8.92 | 16.76 | 15.34 | 36.97 | [67] |
| Hanjiagou | Ag | −14.40 to 0.65 | −10.01 | 17.21 | 15.37 | 37.22 | [67] |
| Pengjiagou | Ag | 4.20 to 8.10 | +5.25 | 16.90 | 15.16 | 37.02 | [67] |
| Lanyan | Ag-Pb-Zn | −10.50 to 0.50 | −5.50 | 16.67 | 15.38 | 37.90 | [10] |
| Changzhuangzi | Ag-Au | 1.50 to 3.00 | +2.10 | 16.34 | 15.19 | 36.22 | [10] |
| Niujuan | Ag-Au | 2.4 to 5.30 | +3.84 | 16.89 | 15.48 | 37.79 | [13] |
| Dongzigou | Ag-Cu-Au | −1.49 to 4.90 | −0.70 | 15.63 | 15.09 | 35.59 | [10] |
| Xiangguang | Ag-Mn | 0.10 to 4.80 | +2.28 | 16.97 | 15.54 | 37.22 | [10] |
| Moguyu | Ag-Cu-Zn | 5.50 to 8.20 | +6.80 | 17.57 | 15.47 | 37.76 | [1] |
| Beichagoumen | Ag-Pb-Zn | 0.20 to 5.20 | +2.94 | 16.57 | 15.02 | 36.25 | [1] |
| Shangluzhouwan | Ag | −4.30 to 1.30 | −0.58 | 16.06 | 14.90 | 36.14 | [1] |
| Bajiazi | Ag-Pb-Zn | −8.20 to 6.70 | +2.90 | 16.27 | 15.23 | 36.46 | [16] |
| Guzigou | Ag-Pb-Zn | 0.89 to 4.32 | +2.68 | 16.37 | 15.20 | 36.43 | [68] |
| Huoshigou | Ag | 5.00 to 11.80 | +8.78 | - | - | - | [10] |
| Chaitun | Ag | 6.4 to 6.9 | +6.70 | - | - | - | [16] |
| Manhantu | Ag-Pb-Zn | - | - | 17.03 | 15.34 | 37.28 | [16] |
| Liujiaying | Ag-Pb-Zn | - | - | 16.38 | 15.22 | 36.73 | [16] |

The lead isotopic compositions of 167 samples from 19 deposits in the YLMB show relatively large variations in the $^{206}Pb/^{204}Pb$, $^{208}Pb/^{204}Pb$, and $^{207}Pb/^{204}Pb$ ratios ranging from 15.63 to 17.57, from 35.59 to 37.79, and from 14.90 to 15.54, respectively (Table 3 and Figure 8). In the lead isotopic evolution diagrams (Figure 8), most data plot between the lower crust and mantle evolution curves, suggesting that the Pb was derived from multiple sources including mantle and the lower crust. The S and Pb isotopic compositions of the sulfides from the Yingfang deposit and other silver polymetallic deposits in this region show marked similarity (Figure 8), suggesting the same or similar lower crustal source with additional mantle input.

Studies of the S and Pb characteristics of silver polymetallic deposits in the northern flank of the NCC suggest similar sources of ore-forming materials implying common geodynamic setting.

### 6.4. The Tectonic Setting and Metallogenic Model

The temporal distribution of the complex Mesozoic mineralization events along the northern flank of the NCC is poorly understood. On the basis of previous studies and the results presented in this study (Table 4), we suggest that the Mesozoic mineralization in the central segment of the northern flank of the NCC can be divided into the following four periods (Figure 10): Middle–Late Triassic (240–205 Ma), Early–Middle Jurassic (190–160 Ma), Late Jurassic (155–135 Ma), and Early Cretaceous (135–100 Ma). In contrast to the northern flank of the NCC, the timing of mineralization in the YLMB is relatively within a narrow interval.

**Table 4.** Ages of ore deposits in the northern flank of the NCC.

| No. | Deposit | Mineralization System | Analytical Methods | Analytical Minerals | Age (Ma) | Reference |
|---|---|---|---|---|---|---|
| 1 | Songbei | Mo | Re-Os | Molybdenite | 184 ± 2.0 | [6] |
| 2 | Xintaimen | Mo | Re-Os | Molybdenite | 183 ± 3.0 | [69] |
| 3 | Lanjiagou | Mo | Re-Os | Molybdenite | 186.5 ± 0.7 | [70] |
| 4 | Yangjiazhangzi | Mo(Pb-Zn) | Re-Os | Molybdenite | 189.7 ± 2.8 | [71] |
| 5 | Bajiazi | Mo(Pb-Zn) | Re-Os | Molybdenite | 204.0 ± 0.5 | [9] |
| 6 | Xiaojiayingzi | Mo(Fe) | Re-Os | Molybdenite | 165.5 ± 4.6 | [9] |
| 7 | Taipingcun | Mo | Re-Os | Molybdenite | 164.110 ± 92 | [72] |
| 8 | Sibozi | Mo(Cu) | Re-Os | Molybdenite | 194 ± 1.0 | [73] |
| 9 | Xiaosigou | Cu(Mo) | Re-Os | Molybdenite | 122.83 ± 2.46 | [70] |
| 10 | Shouwangfen | Cu(Fe, Mo) | Re-Os | Molybdenite | 111 ± 5.3 | [74] |
| 11 | Sadaigoumen | Mo | Re-Os | Molybdenite | 237.0 ± 3.9 | [75] |
| 12 | Dacaoping | Mo | Re-Os | Molybdenite | 137.1 ± 2.6 | [75] |
| 13 | Dazhuangke | Mo | Re-Os | Molybdenite | 137.6 ± 3.7 | [76] |
| 14 | Dawan | Mo(Cu) | Re-Os | Molybdenite | 139.7 ± 6.2 | [70] |
| 15 | Yaojiagou | Mo | Re-Os | Molybdenite | 164.7 ± 2.3 | [77] |
| 16 | Xinling | Mo | Re-Os | Molybdenite | 221.3 ± 3.2 | [77] |
| 17 | Xiaodonggou | Mo | Re-Os | Molybdenite | 135.5 ± 1.5 | [78] |
| 18 | Jiguanshan | Mo | Re-Os | Molybdenite | 151.1 ± 1.3 | [79] |
| 19 | Kulitu | Mo | Re-Os | Molybdenite | 245.0 ± 4.3 | [80] |
| 20 | Nianzigou | Mo | Re-Os | Molybdenite | 154.3 ± 3.6 | [81] |
| 21 | Caosiyao | Mo | Re-Os | Molybdenite | 145.3 ± 1.0 | [82] |
| 22 | Xishadegai | Mo | Re-Os | Molybdenite | 225.4 ± 2.6 | [83] |
| 23 | Dasuji | Mo | Re-Os | Molybdenite | 223.5 ± 5.5 | [84] |
| 24 | Paishanlou | Au | SHRIMP U-Pb | Zircon | 126.1 ± 1.1 | [85] |
| 25 | Siping | Au | Rb-Sr | Quartz | 187 ± 4 | [2] |
| 26 | Jinchanggouliang | Au | Re-Os | Molybdenite | 131.45 ± 0.93 | [86] |
| 27 | Er'daogou | Au | SHRIMP U-Pb | Zircon | 126 ± 2.8 | [87] |
| 28 | Xiaotazigou | Au | LA-ICP-MS U-Pb | Zircon | 239 ± 2 | [88] |
| 29 | Jinchangliang | Au | Re-Os | Molybdenite | 245 ± 1 | [89] |
| 30 | Nailingou | Au | LA-ICP-MS U-Pb | Zircon | 125.5 ± 0.87 | [89] |
| 31 | Jinchangyu | Au | Re-Os | Molybdenite | 242.6 ± 6.8 | [90] |
| 32 | Toudaomenzigou | Au | $^{40}$Ar-$^{39}$Ar | Potash feldspar | 217.3 ± 2.0 | [91] |
| 33 | Shuiquangou | Au | $^{40}$Ar-$^{39}$Ar | Potash feldspar | 212.5 ± 0.4 | [91] |
| 34 | Yuerya | Au | Rb-Sr | Quartz | 168.4 ± 2.7 | [91] |

**Table 4.** *Cont.*

| No. | Deposit | Mineralization System | Analytical Methods | Analytical Minerals | Age (Ma) | Reference |
|---|---|---|---|---|---|---|
| 35 | Tangzhangzi | Au(Mo) | Re-Os | Molybdenite | 170.1 ± 1.6 | [92] |
| 36 | Xiayingfang | Au | Re-Os | Molybdenite | 164.2 ± 2.3 | [93] |
| 37 | Daxigou | Au | LA-ICP-MS U-Pb | Zircon | 136.4 ± 0.7 | [94] |
| 38 | Dongping | Au | LA-ICP-MS U-Pb | Zircon | 186.8 ± 0.3 | [95] |
| 39 | Dongping | Au | $^{40}Ar$-$^{39}Ar$ | Potash feldspar | 177.4 ± 5 | [96] |
| 40 | Zhongshangou | Au | $^{40}Ar$-$^{39}Ar$ | Potash feldspar | 131.45 | [97] |
| 41 | Shuijingtun | Au | $^{40}Ar$-$^{39}Ar$ | Quartz | 115.1 | [2] |
| 42 | Hougou | Au | LA-ICP-MS U-Pb | Zircon | 187.6 ± 0.4 | [98] |
| 43 | Hougou | Au | $^{40}Ar$-$^{39}Ar$ | Potash feldspar | 177.6 ± 1.9 | [99] |
| 44 | Huangtuliang | Au | LA-ICP-MS U-Pb | Zircon | 187.4 ± 0.3 | [95] |
| 45 | Niuxinshan | Au | $^{40}Ar$-$^{39}Ar$ | Quartz | 175.8 ± 3.1 | [100] |
| 46 | Baiyun | Au | Rb-Sr | Sulfides | 225.3 ± 7.0 | [101] |
| 47 | Erdaogou | Au | $^{40}Ar$-$^{39}Ar$ | Quartz | 140.6 ± 2.8 | [87] |
| 48 | Wulong | Au | Rb-Sr | Quartz | 120 ± 3 | [102] |
| 49 | Xiaotongjiabuzi | Au | $^{40}Ar$-$^{39}Ar$ | Sericite | 167 | [103] |
| 50 | Wanquansi | Ag | Rb-Sr | Sulfides | 144.1 ± 4.0 | [104] |
| 51 | Liangjiagou | Ag | Rb-Sr | Sulfides | 126–131.3 | [98] |
| 52 | Niujuan | Ag-Au | Sm-Nd | Fluorite | 139.2 ± 3.8 | [13] |
| 53 | Yingfang | Pb-Zn-Ag | Rb-Sr | Sulfides | 135.7 ± 4.1 | This study |
| 54 | Beichagoumen | Ag-Pb-Zn | LA-ICP-MS U-Pb | Zircon | 138.5 ± 1.3 | [105] |
| 55 | Guzigou | Ag-Pb-Zn | Rb-Sr | Sulfides | 101 ± 4.7 | [24] |
| 56 | Gaojiabuzi | Ag | Rb-Sr | Quartz | 234 ± 14 | [106] |
| 57 | Zhenzigou | Pb-Zn | Rb-Sr | Sphalerite | 221 ± 12 | [107] |
| 58 | Xiquegou | Pb-Zn | Rb-Sr | Pyrite | 225 | [107] |

The tectonic setting evolution of the mineralization in the YLMB is primarily from the closure of the Paleo-Asian Ocean and the formation of the Xing'an-Mongolia Orogenic Belt (XMOB) [108]. The North China-Mongolia plate and the southern margin of the Siberian plate are separated by the Mongolian-Okhotsk Ocean [109]. During Triassic (240–205 Ma), the northern flank of the NCC was in a post-orogenic extensional tectonic setting following the closure of the Paleo-Asian Ocean, which resulted in the lithospheric delamination and asthenosphere upwelling (Figure 11a). This caused extensive volcanism and the emplacement of subvolcanic rocks. Under the influence of the far-field stresses during the extension, the gold and molybdenite mineralization occurred across the XMOB and the NCC coevally with the emplacement of the Triassic felsic or mafic intrusions (Figure 11a) [110].

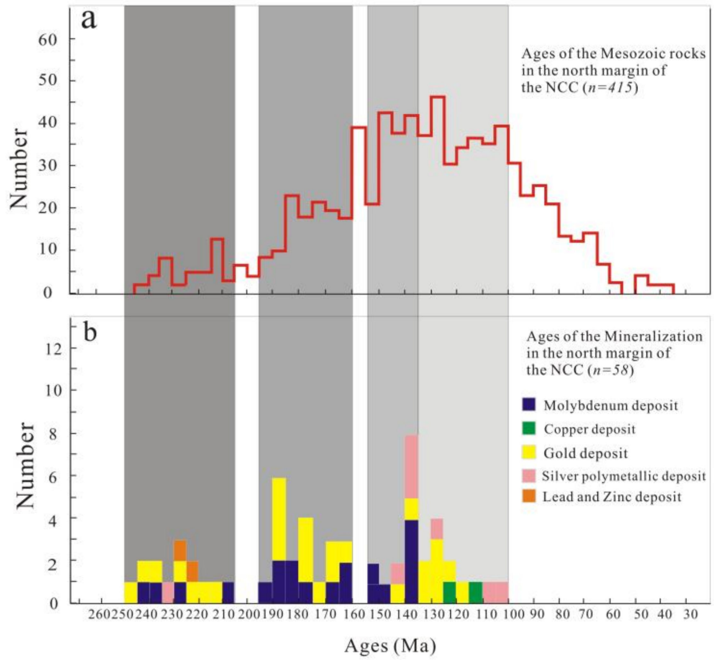


**Figure 10.** The ages of magmatic rocks (**a**) and mineralization (**b**) for the ore deposits on the northern flank of the North China Craton (NCC) (refer to Table 4 for data) formed during the Mesozoic.

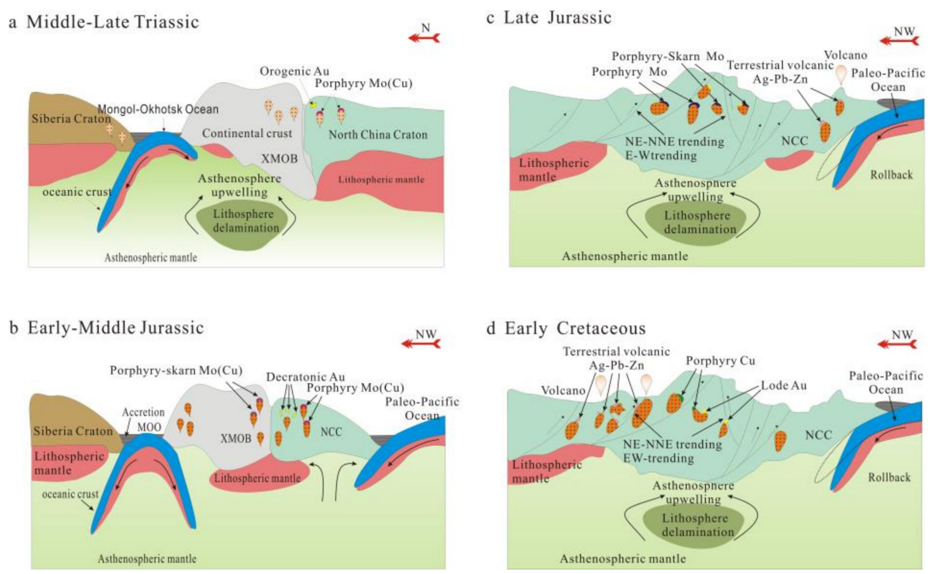


**Figure 11.** Schematic illustration of a genetic model for the mineralization in the northern flank of the NCC during Mesozoic (modified from [96,111]). (**a**) Middle–Late Triassic (240–205 Ma); (**b**) Early–Middle Jurassic (190–160 Ma); (**c**) Late Jurassic (155–135 Ma); (**d**) Early Cretaceous (135–100 Ma). XMOB, Xing'an-Mongolia Orogenic Belt; NCC, North China Craton; MOO, Mongol-Okhotsk Ocean.

The collision between the Siberian Plate and the North China-Mongolia Block might have been ongoing until the closure of the Mongolia-Okhotsk Ocean in the Late Jurassic [25,112–117]. Thus, the effect of the collision between the Siberian Plate and the North China-Mongolia Block on the Early–Mid Jurassic magmatic activity and mineralization episode cannot be excluded in this region [25,66,114]. During Early–Middle Jurassic (190–160 Ma), the geodynamic setting of the northern flank of the NCC was related to the subduction of the Paleo-Pacific plate and the collision between the Siberian Plate and the North China-Mongolia Block (Figure 11b) [96,111]. Widespread volcanism and magmatic activity occurred in the Yanshan–Liaoning area, with associated gold and molybdenite mineralization [118].

During Late Jurassic, influenced by the northwestward subduction of the Paleo-Pacific plate, the regional E–W trending tectonic systems were resurrected and further superposed by NE trending or NNE trending tectonic systems [55,119]. During this period, the adjustment of the lithosphere tectonic regime not only caused volcanic eruption, but also enhanced the mantle–crust interaction, and granitic magmas derived from crustal melting were emplaced at the intersection of the NNE and E–W trending faults, forming syntectonic granodiorite, granite porphyry, adamellite, and syenite [96,117]. Along with the emplacement of the granitic magma, lead, zinc, molybdenum, and copper mineralization formed in association with the I-type or mixed crust-mantle derived granitic magmas, mainly during the end of Late Jurassic (140 $\pm$ 5 Ma) [96,111,120] and produced deposits such as Yingfang deposit in this study. These marked a transformation in the tectonic regime (Figure 11c).

The extensive ore-forming events are considered to be a direct geodynamic consequence of the inhomogeneous lithosphere thinning beneath the NCC. Since the magmatism and mineralization mostly took place in early Cretaceous, large-scale inhomogeneous delamination would also be a feasible model for the thinning of the NCC [2,3]. Following asthenosphere upwelling and lithospheric thinning resulted by the post-collisional extensional environment, the mantle-derived magmas penetrated into the crust, resulting in extensive crustal-reworking and strong interaction between crust and mantle [110,121]. During the lithosphere extension and thinning, magma emplacement and volcanic eruptions were associated with large-scale Mesozoic mineralization in this region [2,3,17,118,122–125]. Different types of ore deposits are widely distributed in the northern flank of the NCC, including skarn copper deposit, quartz vein gold deposit, and volcanic-type silver polymetallic deposits (Figure 11d).

## 7. Conclusions

1. The Rb-Sr isochron age of sulfides from the Yingfang deposit obtained in this study mark the timing of mineralization as 135.7 $\pm$ 4.1 Ma, and the ore-forming materials were primarily derived from crust, with minor input of mantle materials.
2. Mesozoic magmatism and mineralization in the Yingfang deposit mainly took place at 245 and 145–135 Ma. The Pb-Zn-Ag mineralization is related to large-scale inhomogeneous lithosphere thinning beneath the NCC.
3. The silver polymetallic deposits in the YLMB possess similar sources of ore-forming materials.
4. The Mesozoic mineralization events in the northern flank of the NCC can be divided into the following four periods: 240–205 Ma, 190–160 Ma, 155–135 Ma, and 135–100 Ma.

**Author Contributions:** Supervision, L.L., S.L. and M.S.; experiments and analysis, X.L. and Y.L. writing—original draft, X.L.; writing—review and editing, X.L and S.L. All authors have read and agreed to the published version of the manuscript.

**Funding:** Ministry of Science and Technology of the People's Republic of China, 2016YFC0600106 and the China Geological Survey, 12120114051101.

**Institutional Review Board Statement:** Not applicable.

**Informed Consent Statement:** Not applicable.

**Data Availability Statement:** Data available in a publicly accessible repository.

**Acknowledgments:** We are grateful to the staff in the Fengning Yanshan Mining Limited Liability Company for their help during field work. We also thank Master Course students of our team from the China University of Geosciences Beijing for their support during our laboratory work. This work was supported by the Ministry of Science and Technology of the People's Republic of China (2016YFC0600106) and China Geological Survey (12120114051101).

**Conflicts of Interest:** The authors declare no conflict of interest.

## References


1. Mao, D.B.; Zhong, C.T.; Chen, Z.H.; Hu, X.D. On the metollogenic aspects of Pb-Zn-Ag deposits in the middle north flank of north china block. *Prog. Precambrian Res.* **2002**, *25*, 105–112, (In Chinese with English abstract).
2. Li, S.R.; Santosh, M. Metallogeny and craton destruction: Records from the North China Craton. *Ore Geol. Rev.* **2014**, *56*, 376–414. [CrossRef]
3. Li, S.R.; Santosh, M. Geodynamics of heterogeneous gold mineralization in the North China Craton and its relationship to lithospheric destruction. *Gondwana Res.* **2017**, *50*, 267–292. [CrossRef]
4. Chen, Y.C.; Xue, C.J.; Wang, D.H.; Li, H.Q.; Lu, Y.F. A discussion on the regional mineralizing pedigree of the ore deposits in the northern flank of the North China. *Geol. J. China Univ.* **2003**, *9*, 520–535, (In Chinese with English abstract).
5. Peng, R.M.; Zhai, Y.S. Hydrothermal Mineralization on the Mesoproterozoic Passive Continental Flanks of China: A Case Study of the Langshan-Zhaertaishan Belt, Inner Mongolia, China. *Acta Geol. Sin.* **2004**, *78*, 534–547.
6. Chu, S.; Zeng, Q.; Liu, J. Re-Os and U-Pb geochronology of the Songbei porphyry-skarn Mo deposit, North China Craton: Implications for the Early Jurassic tectonic setting in eastern China. *J. Geochem. Explor.* **2017**, *181*, 256–269. [CrossRef]
7. Zhao, G.C.; Cawood, P.A.; Wilde, S.A.; Sun, M.; Lu, L.Z. Metamorphism of basement rocks in the Central Zone of the North China Craton: Implications for Paleoproterozoic tectonic evolution. *Precambrian Res.* **2000**, *103*, 55–88. [CrossRef]
8. Santosh, M. Assembling North China Craton within the Columbia supercontinent: The role of double-sided subduct ion. *Precambrian Res.* **2010**, *178*, 149–167. [CrossRef]
9. Dai, J.Z.; Mao, J.W.; Zhao, C.; Xie, G.; Yang, F.; Wang, Y. New U-Pb and Re-Os age data and the geodynamic setting of the Xiaojiayingzi Mo (Fe) deposit, western Liaoning province, Northeastern China. *Ore Geol. Rev.* **2009**, *35*, 235–244. [CrossRef]
10. Yang, S.D. Ore Forming Geological Characteristics and Scientific Prospecting for Silver Deposits in North Hebei Province. Ph.D. Thesis, Central South University of Technology, Guangzhou, China, 2000. (In Chinese with English abstract).
11. Li, J.M. Silver Deposits and Their Metallogenic Geodynamics Setting in Yanshan Area. Ph.D. Thesis, Northeastern University, Shenyang, China, 2006. (In Chinese with English abstract).
12. Li, J.M.; Ye, Q.; Liu, W.J.; Wang, Z. Discussion on metallogenic regularities and dynamics of Mesozoic endogenous non-ferrous metals of Northern Hebei. *Miner. Resour. Geol.* **2011**, *25*, 98–104, (In Chinese with English abstract).
13. Li, Y.J.; Li, S.R.; Mo, X.X.; Santosh, M. Isotope geochemistry and geochronology of the Niujuan silver deposit, northern North China Craton: Implications for magmatism and metallogeny in an extensional tectonic setting. *Ore Geol. Rev.* **2017**, *90*, 36–41. [CrossRef]
14. Shen, L.X.; Li, W.S.; Wang, Z.L.; Ma, J.X.; Li, C.Y. Forecast for the deep mineralization of niujuan silver-gold deposit and yingfang silver-lead-zinc deposit in northern hebei province. *Contrib. Geol. Miner. Resour. Res.* **2012**, *4*, 450–457, (In Chinese with English abstract).
15. Yan, X.; Chen, B.; Duan, X.X.; Wang, Z.Q. Geochronology and Ore Genesis of the Niujuan-Yingfang Pb-Zn-Ag Deposit in Fengning, Northern North China Craton: Constraints from Fluid Inclusions, H-O-S Isotopes and Fluorite Sr-Nd Isotopes. *J. Asian Earth Sci.* **2021**, *32*, 81–102. (In Chinese)
16. Quan, H.; Han, Q.Y.; Ai, Y.F.; Lin, Y.C. *The Features and Prospects of Metallogenesis of Polymetals, Gold and Silver in Yan-Liao Area of China*; Geology Publishing House: Beijing, China, 1992; pp. 59–72. (In Chinese)
17. Li, C.; Zhang, C.; Cope, T.D.; Lin, Y. Out-of-sequence thrusting in polycyclic thrust belts: An example from the mesozoic Yanshan belt, North China Craton: Out-of-sequence thrusting in the Yanshan. *Tectonics* **2016**, *35*, 2082–2116. [CrossRef]
18. Zhu, R.; Xu, Y.; Zhu, G.; Zhang, H.; Xia, Q.; Zheng, T. Destruction of the north China Craton. *Sci. China Earth Sci.* **2012**, *55*, 1565–1587. [CrossRef]
19. Zhang, H.F.; Zhu, R.X.; Santosh, M.; Ying, J.F.; Su, B.X.; Hu, Y. Episodic widespread magma underplating beneath the North China Craton in the Phanerozoic: Implications for craton destruction. *Gondwana Res.* **2013**, *23*, 95–107. [CrossRef]
20. Mao, D.B.; Zhong, C.T.; Chen, Z.H.; Hu, X.D. Structural analysis of metallogenic geological attributes for Pb-Zn-Ag deposits in northern Hebei province. *Earth Sci. J. China Univ. Geosci.* **1999**, *24*, 464–467, (In Chinese with English abstract).
21. Wang, L.J.; Wang, J.B.; Wang, Y.W.; Zhu, H.P. Study of metallic fluid of caijiaying Pb-Zn-Ag Deposit. *Miner. Depos.* **2002**, *21*, 1037–1040, (In Chinese with English abstract).
22. Chen, W.J.; Liu, H.T.; Zhang, D.H. Fluid inclusion's characteristics of the Niujuan silve deposit in Fengning, Hebei, and its geological significance. *Miner. Resour. Geol.* **2007**, *4*, 36–40, (In Chinese with English abstract).
23. Li, Z.Y.; Liu, X.Y.; Li, S.M.; Hu, H.B.; Yang, Y. An analysis of geological age and materials source of the Niujuan Ag-Au polymetallic deposit in Chengde. *Geol. China* **2014**, *41*, 951–960, (In Chinese with English abstract).
24. Wang, J.; Chen, F.H.; Liu, H.L.; Zhao, Y.C.; Xie, L.; Xie, G.Q. Rb-Sr Isochron Ages of the Guzigou Pb-Zn-Ag Ore Deposits in the Chengde area, northern Hebei province. *Miner. Depos.* **2014**, *33*, 271–272. (In Chinese)
25. Davis, G.A.; Zheng, Y.D.; Wang, C. Mesozoic tectonic evolution of the Yanshan folds and thrust belt, with emphasis on Hehei and Liaoning Provinces, Northern China. *GSA Memoir.* **2001**, *194*, 171–197.
26. Quan, H. Nonferrous metallic deposits in the northern Hebei Province–western Liaoning Province area. In *Geology and Nonferrous Metallic Deposits in the Northern Flank of the North China Landmass and Its Adjacent*; Rui, Ed.; Geological Publishing House: Beijing, China, 1994; pp. 383–471. (In Chinese)

27. Zhu, D.G.; Wu, Z.H.; Cui, S.Q. Features of Mesozoic magmatic activities in the Yanshan area and their relations to intracontinental orogenesis. *Geol. Rev.* **1999**, *45*, 163–172, (In Chinese with English abstract).
28. Ma, Y.C.; Wang, C.G.; Feng, G.Q.; Li, Y.Q.; Song, Y.C.; Jia, G.N. Prospecting of Yangjiazhangzi ore deposit area. *Miner. Depos.* **2002**, *21*, 435–438. (In Chinese)
29. Liu, X.L.; Fan, P.; Zheng, Z.F.; Li, A.L. The Yangjiazhangzi-Bajiazi molybdenumpolymetal metallogenic belt in western Liaoning province: Characteristics of typical molybdenum deposits and prediction for exploration. *Geol. Resour.* **2009**, *18*, 110–115, (In Chinese with English abstract).
30. Wong, W.H. The Mesozoic orogenic movements in eastern China. *Geol. Bull. China* **1929**, *8*, 33–44. (in Chinese). [CrossRef]
31. Zhao, Y. The Mesozoic orogenic and tectonic evolution of the Yanshan area. *Geol. Rev.* **1990**, *36*, 1–13, (In Chinese with English abstract).
32. Zhao, Y.; Zhang, S.H.; Xu, G.; Yang, Z.Y.; Hu, J.M. The Jurassic major tectonic events of the Yanshanian intraplate deformation belt. *Geol. Bull. China* **2004**, *23*, 854–862. (In Chinese)
33. Wang, Y.X.; Yang, J.D.; Chen, J. The Sr and Nd isotopic variations of the Chinese Loess Plateau during the past 7 Ma: Implications for the East Asian winter monsoon and source areas of loess. *Palaeogeogr. Palaeoclimatol. Palaeoecol.* **2007**, *249*, 351–361. [CrossRef]
34. Giesenmann, A.; Jäger, H.J.; Norman, A.L.; Krouse, H.R.; Brand, W.A. On-line sulfur-isotope determination using an elemental analyser coupled to a mass spectrometer. *Anal. Chem.* **1994**, *66*, 2816–2819. [CrossRef]
35. Ludwig, K.R. *User's Manual for Isoplot/EX Version 3.0. A Geochronological Toolkit for Microsoft Excel*; Berkeley Geochronology Center: Berkeley, CA, USA, 2003; Volume 4, pp. 1–71.
36. Shepherd, T.; Darbyshire, D. Fluid inclusion Rb–Sr isochrons for dating mineral deposits. *Nature* **1981**, *290*, 578–579. [CrossRef]
37. Brannon, J.C.; Podosek, F.A.; Mclimans, R.K. Alleghenian age of the Upper Mississippi Valley zinc-lead deposit determined by Rb-Sr dating of sphalerite. *Nature* **1992**, *356*, 509–511. [CrossRef]
38. Nakai, S.; Halliday, A.N.; Kesler, S.E.; Jones, H.D.; Kyle, J.R.; Lane, T.E. Rb–Sr dating of sphalerites from Mississippi Valley-type (MVT) ore deposits. *Geochim. Cosmochim. Acta* **1993**, *57*, 417–427. [CrossRef]
39. Li, Q.L.; Chen, F.K.; Yang, J.H.; Fan, H.R. Single grain pyrite Rb-Sr dating of the Linglong gold deposit, eastern China. *Ore Geol. Rev.* **2008**, *34*, 263–270. [CrossRef]
40. Li, T.G.; Wu, G.; Liu, J.; Hu, Y.Q.; Zhang, Y.F.; Luo, D.F. Rb-Sr isochron age of the Jiawula Pb-Zn-Ag deposit in the Manzhouli area and its geological significance. *Acta Petrol. Sin.* **2014**, *30*, 257–270, (In Chinese with English abstract).
41. Sun, W.Y.; Li, S.R.; Santosh, M.; Wang, X.; Zhang, L.J. Isotope geochemistry and geochronology of the Qiubudong silver deposit, central North China Craton: Implications for ore genesis and lithospheric dynamics. *Ore Geol. Rev.* **2014**, *57*, 229–242. [CrossRef]
42. Ni, P.; Wang, G.G.; Chen, H.; Xu, Y.F.; Guan, S.J.; Pan, J.Y. An Early Paleozoic orogenic gold belt along the Jiang-Shao Fault, South China: Evidence from fluid inclusions and Rb-Sr dating of quartz in the Huangshan and Pingshui deposits. *J. Asian Earth Sci.* **2015**, *103*, 87–102. [CrossRef]
43. Ma, Y.B.; Bagas, L.; Xing, S.W.; Zhang, S.T.; Wang, R.J.; Li, N.; Wang, Y.; Wang, Y.; Zhang, Z.-J.; Zou, Y.-F.; et al. Genesis of the stratiform Zhenzigou Pb, Zn deposit in the North China Craton: Rb-Sr and C-O-S-Pb isotope constraints. *Ore Geol. Rev.* **2016**, *79*, 88–104. [CrossRef]
44. Li, L.; Li, S.R.; Santosh, M.; Zhu, J.; Suo, X.J. Early Jurassic decratonic gold metallogenesis in the Eastern North China Craton: Constraints from S-Pb-C-D-O isotopic systematics and pyrite Rb-Sr geochronology of the Guilaizhuang Te-Au deposit. *Ore Geol. Rev.* **2018**, *92*, 558–568. [CrossRef]
45. Zeng, Y.J.; Li, L.; Li, S.R.; Santosh, M.; Song, Y.X.; Alam, M. Rb–Sr geochronology and geochemistry of pyrite from the Shihu gold deposit, central North China Craton: Implication for the timing and genesis of gold mineralization. *Geol. J.* **2020**, *55*, 5779–5790. [CrossRef]
46. Li, W.B.; Huang, Z.L.; Xu, D.R.; Chen, J.; Xu, C.; Guan, T. Rb–Sr isotopic method on zinc–lead ore deposits: A review. *Geotect. Metall.* **2002**, *26*, 436–441, (In Chinese with English abstract).
47. Seal, R.R. Sulfur isotope geochemistry of sulfide minerals. *Rev. Mineral. Geochem.* **2006**, *61*, 633–677. [CrossRef]
48. Sakai, H. Isotopic properties of sulfur compounds in hydrothermal processes. *Geochem. J.* **1968**, *2*, 29–49. [CrossRef]
49. Ohmoto, H.; Rye, R.O. Isotopes of sulfur and carbon. In *Geochemistry of Hydrothermal Ore Deposits*; Barnes, H.L., Ed.; Wiley: New York, NY, USA, 1979; pp. 509–567.
50. Hoefs, J. *Stable Isotope Geochemistry*, 3rd ed.; Springer: Berlin/Heidelberg, Germany, 1997; pp. 1–201.
51. Ohmoto, H. Systematics of sulfur and carbon isotopes in hydrothermal ore deposits. *Econ. Geol.* **1972**, *67*, 551–578. [CrossRef]
52. Wu, G.; Chen, Y.C.; Li, Z.Y.; Liu, J.; Yang, X.S.; Qiao, C.J. Geochronology and fluid inclusion study of the Yinjiagou porphyry-skarn Mo-Cu-pyrite deposit in the East Qinling orogenic belt, China. *J. Asian Earth Sci.* **2014**, *79*, 585–607. [CrossRef]
53. Ohmoto, H. Stable isotope geochemistry of ore deposits. *Rev. Mineral. Geochem.* **1986**, *16*, 491–559.
54. Zheng, Y.F.; Chen, J.F. *Geochemistry of Stable Isotopes*; Science Press: Beijing, China, 2000; pp. 1–316. (In Chinese)
55. Xu, Z.C.; Wang, Z.M. Geotectonic features of Yanshan area in Hebei province. *Reg. Geol. Chin.* **1983**, *3*, 39–55, (In Chinese with English abstract).
56. Kiyosu, Y. Sulfur isotopic fractionation among sphalerite, galena and sulfide ions. *Geochem. Soc. Jpn.* **1973**, *7*, 191–199. [CrossRef]
57. Saravanan, C.S.; Mishra, B. Uniformity in sulfur isotope composition in the orogenic gold deposits from the Dharwar Craton, southern India. *Miner. Depos.* **2009**, *44*, 597–605. [CrossRef]
58. Faure, G. *Principles of Isotope Geology*, 2nd ed.; Wiley Interscience: New York, NY, USA, 1986; pp. 22–70.

59. Hu, X.W.; Zhang, J.M.; Quan, H. The isotopic age of the Hongqiyingzi group in North Hebei province. *Reg. Geol. China* **1996**, *2*, 186–192. (In Chinese)
60. Stacey, J.S.; Kramers, J.D. Approximation of terrestrial lead isotope evolution by a two-stage model. *Earth Planet. Sci. Lett.* **1975**, *26*, 207–221. [CrossRef]
61. Zartman, R.E.; Doe, B.R. Plumbotectonic—The model. *Tectonophysics* **1981**, *75*, 135–162. [CrossRef]
62. Doe, B.R.; Zartman, R.E. Plumbotectonics of the phanerozoic. In *Geochemistry of Hydrothermal Ore Deposits*; Barnes, H.L., Ed.; John Wiley: New York, NY, USA, 1979; pp. 22–70.
63. Hou, M.L.; Jiang, S.Y.; Jiang, Y.H.; Ling, H.F. S-Pb isotope geochemistry and Rb-Sr geochronology of the Penglai gold field in the eastern Shandong Province. *Acta Petrol. Sin.* **2006**, *22*, 2525–2533, (In Chinese with English abstract).
64. Sun, S.L. The Study on Metallogenic Series of Hydrocarbon Alkali-Fluids in Devonian in Xicheng Concentrated Mineralization Area, West Qinling, Gansu Province. Ph.D. Thesis, Chengdu University of Technology, Chengdu, China, 2001; pp. 43–44, (In Chinese with English abstract).
65. Wang, B.D.; Niu, S.Y.; Sun, A.Q.; Zhang, J.Z. *Deep Sources of Ore-Forming Materials and the Metallogenesis of Mantle Branch Structure*; Geological Publishing House: Beijing, China, 2010; pp. 1–256.
66. Shen, J.F.; Santosh, M.; Li, S.R. He-Ar, S, Pb and O isotope geochemistry of the Dabaiyang gold deposit: Implications for the relationship between gold metallogeny and destruction of the North China Craton. *Ore Geol. Rev.* **2020**, *116*, 103229. [CrossRef]
67. Song, R.X.; Wang, Y.Z. *Geology of Gold Ore Deposits in Hebei*; Geological Publishing House: Beijing, China, 1994. (In Chinese)
68. Chen, C.L.; Liu, X.Y.; Tong, W.J. The geological characteristics and causes of the Guzigou silver polymetallic ore deposit in Chengde. *Earth* **2015**, *6*, 50–52, (In Chinese with English abstract).
69. Zhang, Z.Z.; Changzhi, W.U.; Lianxing, G.U.; Hui, F.; Zheng, Y.C.; Huang, J.H. Molybdenite Re-Os dating of Xintaimen molybdenum deposit in Yanshan-Liaoning metallogenic belt, North China. *Miner. Depos.* **2009**, *28*, 313–320, (In Chinese with English abstract).
70. Huang, D.H.; Du, A.D.; Wu, C.Y.; Liu, L.S.; Sun, Y.L.; Zou, X.Q. Geochronology of molybdenum (copper) deposits in the north China platform: Re-Os age of molybdenite and its geological significance. *Miner. Depos.* **1996**, *15*, 289–297, (In Chinese with English abstract).
71. Chu, S.X. Structure-magma-fluid Evolution and Mineralization of Yangjiazhangzi Molybdenum Ore Field in the Eastern Segment of Yan-liao Molybdenum Metallogenic Belt. Ph.D. Thesis, Institute of Geology and Geophysics, Chinese Academy of Sciences, Beijing, China, 2011. (In Chinese with English abstract).
72. Sun, J.L.; Ren, Y.S.; Yang, Y.S.; Wang, Q.; Liu, J.B.; Zhang, J.J.; Nie, W.D.; Wang, A.C.; Qu, W.J. Re-Os isotopic dating of molybdenite from Taipingcun Mo deposit in eastern Hebei and its geological significance. *Glob. Geol.* **2016**, *35*, 738–751, (In Chinese with English abstract).
73. Li, Q.; Meng, X.Y.; Wu, F. LA-ICP-MS zircon U-Pb dating of intrusive rocks and its metallogenic significance in Sibozi-Liubozi molybdenum-copper deposit of Qinglong County, Hebei Province. *Miner. Depos.* **2012**, 255–270, (In Chinese with English abstract).
74. Zhang, R.B.; Liu, J.M.; Ye, J.; Chen, F.K. Chalcopyrite Rb-Sr isochron age dating and its' ore-forming significance in Shouwangfen copper deposit, Hebei province. *Acta Petrol. Sin.* **2008**, *24*, 1353–1358, (In Chinese with English abstract).
75. Duan, H.C.; Qin, Z.Y.; Lin, X.H.; Zhang, B.H.; Liu, X.B.; Zhang, X.; Guo, P.Z.; Han, F.; Qin, L.; Dai, J.Z. Zircon U-Pb ages of intrusive bodies in Dacaoping molybdenum ore district, Fengning Country, Hebei province. *Miner. Depos.* **2007**, *26*, 634–642, (In Chinese with English abstract).
76. Liu, S.B.; Li, C.; Ceng, K.; Qu, W.J. Re-Os dating for molybdenite-bearing rock samples: Application in Dazhuangke molybdenum deposit in Beijing. *Geoscience* **2012**, *26*, 254–260, (In Chinese with English abstract).
77. Liu, X.Y. Metallogenic Model and Prospecting Direction Research of Qingchengzi Polymetallic Ore Field in Liaoning Province. Ph.D. Thesis, China University of Geosciences, Beijing, China, 2020. (In Chinese with English abstract).
78. Nie, F.J.; Jiang, S.H.; Liu, Y.; Zhang, Y. Sm-Nd isotopes of metamorphic volcanic rocks in the Qiaogou area of Beishan, Inner Mongolia. *Acta Geol. Sin.* **2004**, *6*, 807–812. (In Chinese)
79. Chen, W.J.; Liu, J.M.; Liu, H.T.; Sun, X.G.; Zhang, R.B.; Zhang, Z.L.; Qin, F. Study on ore-forming age and ore-forming fluid of Jiguanshan porphyry molybdenum deposit in Inner Mongolia. *Acta Petrol. Sin.* **2010**, *26*, 1423–1436. (In Chinese)
80. Sun, Y.; Liu, J.M.; Zeng, Q.D.; Chu, S.X.; Zhou, L.L.; Wu, G.B.; Gao, Y.Y.; Shen, W.J. Geological characteristics and molybdenite re-os age of Baituyingzi molybdenum copper deposit in eastern Inner Mongolia and its significance. *Acta Petrol. Sin.* **2013**, *29*, 241–254. (In Chinese)
81. Zhang, Z.L.; Zeng, Q.D.; Qu, W.J.; Liu, J.M.; Sun, X.G.; Zhang, R.B.; Chen, W.J.; Qin, F. Re-Os isotope age of molybdenite from Nianzigou molybdenum deposit in Inner Mongolia and its geological significance. *Acta Petrol. Sin.* **2009**, *25*, 212–218. (In Chinese)
82. Fan, H.Y.; Li, T.G.; Wu, W.H. Geochronology of Mo-Pb-Zn-Au mineralization system of Caosiyao superlarge porphyry in Xinghe County, Inner Mongolia and its geological significance. *Miner. Depos.* **2018**, *37*, 355–370. (In Chinese)
83. Zhang, Y.M.; Gu, X.X.; Dong, S.Y.; Cheng, W.B.; Huang, Z.Q.; Li, F.L.; Yang, W.L. Zircon U-Pb and molybdenite Re-Os ages of Xishadegai molybdenum deposit in Inner Mongolia and their geological significance. *Mineral. Petrol.* **2011**, *31*, 33–41. (In Chinese)
84. Wu, H.; Wu, G.; Tao, H.; Wang, G.R.; Li, T.G.; Chen, J.Q.; Yang, N.N. Re_Os Isotope Age and Fluid Inclusion of Molybdenite in Dasuji Porphyry Molybdenum Deposit, Zhuozi County. *Inn. Mong. Miner. Depos.* **2014**, *33*, 1251–1267. (In Chinese)

85. Wang, R.H.; Jin, C.Z.; Li, L.C. $^{40}$Ar-$^{39}$Ar Isotopic Dating for Paishanlou Gold Deposit and its Geological Implication. *J. Northeast. Univ.* **2008**, *29*, 1482–1485, (In Chinese with English abstract).
86. Hou, W.R. Contrast Study on Hadamengou Gold Deposit and Jinchanggouliang Gold Deposit, Inner Mongolia. Ph.D. Thesis, Chinese Academy of Geological Sciences, Beijing, China, 2011. (In Chinese with English abstract).
87. Miao, L.C.; Fan, W.M.; Zhai, M.G. Zircon SHRIMP U-Pb geochronology of the granitoid intrusions from Jinchanggouliang-Erdaogou gold orefield and its significance. *Acta Petrol. Sin.* **2003**, *19*, 71–80, (In Chinese with English abstract).
88. Song, W.M.; Xing, D.H.; Guo, S.Z.; Peng, Y.D.; Bian, X.F.; Tao, N. Lithogeochemistry and significance of the Xiduimiangou rock body in Jinchanggouliang, Inner Mongolia. *Geol. Resour.* **2009**, *18*, 134–139, (In Chinese with English abstract).
89. Sun, Z.J. Study on Gold Deposits Mineralization in Chifeng-Chaoyang Region, Northern Flank of North Craton. Ph.D. Thesis, Jilin University, Changchun, China, 2013.
90. Song, Y.; Wang, R.J.; Nie, F.J.; Hu, J.Z.; Shi, C.L.; Zhang, S. Discovery of Indosinian Mineralization and Its Geological Significance in Jinchangyu Gold Deposit, eastern Hebei Province. *Acta Geosci. Sin.* **2011**, *32*, 125–128. (In Chinese)
91. Chen, S.C.; Ye, H.S.; Wang, Y.T.; Zhang, X.K.; Lu, D.Y.; Hu, H.B. Re-Os age of molybdenite from the Yu'erya Au deposit in eastern Hebei province and its geological significance. *Geol. China* **2014**, *41*, 1565–1576, (In Chinese with English abstract).
92. Li, Z.Y.; Ye, H.S.; He, W. Geological characteristics and molybdenite Re-Os isotopic dating of Tangzhangzi gold (molybdenum) deposit in eastern Hebei Province. *Miner. Depos.* **2014**, *33*, 1366–1378, (In Chinese with English abstract).
93. Zou, T.; Wang, Y.W.; Wang, J.B.; Zhang, H.Q.; Zhao, L.T.; Xie, H.J. Geochronology of the Xiayingfang Au deposit in eastern Hebei province. *Geol. Explor.* **2016**, *52*, 84–97, (In Chinese with English abstract).
94. Jiang, Z.; Jiang, S.; Liu, Y.; Jinxing, B.O.; Chen, J. Geochronology of main intrusive rocks in Daxigou gold deposit, northern Hebei province and their tectonic-metallogenic singnificane. *Acta Geol. Sin.* **2016**, *90*, 1817–1834.
95. Jiang, S.H.; Nie, F.J. $^{40}$Ar/$^{39}$Ar geochronology study on the alkaline intrusive complex and related gold deposits, northwestern Hebei, China. *Geol. Rev.* **2000**, *46*, 621–627, (In Chinese with English abstract).
96. Mao, J.W.; Wang, Y.T.; Zhang, Z.H.; Yu, J.J.; Niu, B.G. Geodynamic settings of Mesozoic large-scale mineralization in the North China and adjacent areas: Implication from the highly precise and accurate ages of metal deposits. *Sci. China Ser. D* **2003**, *46*, 838–851. [CrossRef]
97. Hart, C.J.; Goldfarb, R.J.; Qiu, Y.; Snee, L.; Miller, L.D.; Miller, M.L. Gold deposits of the northern flank of the North China Craton: Multiple late Paleozoic-Mesozoic mineralizing events. *Miner. Depos.* **2002**, *37*, 326–351. [CrossRef]
98. Li, C.M.; Li, T.; Deng, J.F.; Su, S.G.; Liu, X.M. LA-ICP-MS zircon U-Pb age of the brittle-ductile shear zones in Hougou gold orefield, NW Hebei Province. *Geotecton. Metallog.* **2012**, *36*, 157–167, (In Chinese with English abstract).
99. Hu, D.X.; Luo, G.L. $^{40}$Ar/$^{39}$Ar ages of gold-bearing quartz veins and their geological significance in typical gold deposits of Zhangjiakou-Xuanhua gold field, Hebei province. *Sci. Geol. Sin.* **1994**, *29*, 151–158, (In Chinese with English abstract).
100. Guo, S.F.; Tang, Z.L.; Luo, Z.H.; Zhao, W.H. Zircon SHRIMP U-Pb dating of the Tangzhangzi and Niuxinshan granites in eastern Hebei Province and its geological significance. *Geol. Bull. China* **2009**, *10*, 1458–1464. (In Chinese)
101. Zhang, P.; Li, B.; Li, J.; Chai, P.; Wang, X.J.; Sha, D.M.; Shi, J.M. Re-Os dating of pyrite and its geological significance in Baiyun gold deposit, Liaodong rift valley. *Geotecton. Metallog.* **2016**, *40*, 731–738. (In Chinese)
102. Wei, J.H.; Liu, C.Q.; Li, Z.D.; Zhao, Y.X. On the determination of metallogenic age of gold deposits: A case study of Rb-Sr and U-Pb isotopic age of diagenesis and mineralization in Dandong area. *Acta Geol. Sin.* **2003**, *1*, 113–119. (in Chinese).
103. Liu, G.P.; Ai, Y.F. Discussion on the metallogenic age of Xiaotongjiapuzi gold deposit, Liaoning Province. *Miner. Depos.* **2002**, *21*, 53–57. (In Chinese)
104. Liu, Q.M.; Han, Y.C.; Li, S.M. Formation age and geological significance of Wanquansi silver-gold deposit in Chicheng county, Hebei province. *Acta Geosci. Sin.* **2018**, *39*, 474–480.
105. Chen, Z.H.; Mao, D.B.; Zuo, Y.C.; Li, H.M.; Zhong, C.D.; Xiang, Z.Q. Mesozoic intrusive magmatism-related metallogenetic system in Beichagoumen area. *Acta Petrol. Sin.* **2004**, *25*, 224–228, (In Chinese with English abstract).
106. Xue, C.J.; Chen, Y.C.; Lu, Y.F.; Li, H.Q. Metallogenic epochs of Au and Ag deposits in Qingchengzi ore-clustered area, eastern Liaoning Province. *Miner. Depos.* **2003**, *22*, 177–184. (In Chinese)
107. Yu, G.; Chen, J.F.; Xue, C.J. Geochronological framework and Pb, Sr isotope geochemistry of the Qingchengzi Pb–Zn–Ag–Au orefield, Northeastern China. *Ore Geol. Rev.* **2009**, *35*, 367–382. [CrossRef]
108. Wu, F.Y.; Sun, D.Y.; Ge, W.C.; Zhang, Y.B.; Grant, M.L.; Wilde, S.A.; Jahn, B.M. Geochronology of the Phanerozoic granitoids in northeastern China. *J. Asian Earth Sci.* **2011**, *41*, 1–30. [CrossRef]
109. Ren, J.S. *Geological Characteristics and Metallogenic Prediction of the Continental Lithosphere in East China and Its Adjugating Areas*; Science Press: Beijing, China, 1990. (In Chinese)
110. Yang, J.H.; Wu, F.Y.; Wilde, S.A. A review of the geodynamic setting of large-scale late mesozoic gold mineralization in the north china craton: An association with lithospheric thinning. *Ore Geol. Rev.* **2003**, *23*, 125–152. [CrossRef]
111. Mao, J.W.; Xie, G.Q.; Zhang, Z.H.; Li, X.F.; Wang, Y.T.; Zhang, C.Q.; Li, Y.F. Mesozoic large-scale metallogenic pulses in North China and corresponding geodynamic settings. *Acta Petrol. Sin.* **2005**, *21*, 169–188.
112. Li, J.Y. Some new ideas on tectonics of NE China and its neighboring areas. *Geol. Rev.* **1998**, *44*, 339–347. (In Chinese)
113. Zorin, Y.A. Geodynamics of the western part of the Mongolia-Okhotsk collisional belt, Trans-Baikal region (Russia) and Mongolia. *Tectonophysics* **1999**, *306*, 33–56. [CrossRef]

114. Davis, G.A.; Wang, C.; Zheng, Y.D.; Zhang, J.J.; Zhang, C.H.; Gehrels, G.E. The enigmatic Yinshan fold-and-thrust belt of northern China: New views on its intraplate contractional styles. *Geology* **1998**, *26*, 43–46. [CrossRef]
115. Meng, Q.R. What drove late Mesozoic extension of the northern China-Mongolia tract? *Tectonophysics* **2003**, *369*, 155–174. [CrossRef]
116. Deng, J.F.; Zhao, G.C.; Su, S.G.; Liu, C.; Chen, Y.H.; Li, F.N.; Zhao, X.G. Structure overlap and tectonic setting of Yanshan orogenic belt in Yanshan area. *Geotecton. Metallog.* **2005**, *29*, 157–165, (In Chinese with English abstract).
117. Jahn, B.M.; Litvinovsky, B.A.; Zanvilevich, A.N.; Reichow, M. Peralkaline granitoid magmatism in the Mongolian–Transbaikalian Belt: Evolution, petrogenesis and tectonic significance. *Lithos* **2009**, *113*, 521–539. [CrossRef]
118. Zhang, L.C.; Bai, Y.; Zhu, M.T.; Huang, K.; Peng, Z. Regional heterogeneous temporal–spatial distribution of gold deposits in the North China Craton: A review. *Geol. J.* **2020**, *55*, 5646–5663. [CrossRef]
119. Yin, A.; Nie, S. A Phanerozoic palin spastic reconstruction of China and its neighboring regions. In *The Tectonic Evolution of Asia*; Yin, A., Harrison, T.A., Eds.; Cambridge University Press: New York, NY, USA, 1996; pp. 442–485.
120. Pei, R.F.; Lu, F.X.; Fan, J.Z. *Metallogenic Series and Prospecting of the Metal Deposits in North Flank of the North China Craton*; Geological Publishing House: Beijing, China, 1998; pp. 1–237. (In Chinese)
121. Yang, Q.Y.; Santosh, M. The building of an Archean microcontinent: Evidence from the North China Craton. *Gondwana Res.* **2017**, *50*, 3–37. [CrossRef]
122. Wu, F.Y.; Jahn, B.M.; Wilde, S.A.; Lo, C.H.; Yui, T.F.; Lin, Q.; Ge, W.C.; Sun, D.Y. Highly fractionated I-type granites in NE China (I): Geochronology and petrogenesis. *Lithos* **2003**, *66*, 241–273. [CrossRef]
123. Wu, F.Y.; Lin, J.Q.; Wilde, S.A.; Zhang, X.O.; Yang, J.H. Nature and significance of the Early Cretaceous giant igneous event in eastern China. *Earth Planet. Sci. Lett.* **2005**, *233*, 103–119. [CrossRef]
124. Zhu, R.X.; Chen, L.; Wu, F.Y.; Liu, J.L. Timing, scale and mechanism of the destruction of the North China Craton. *Sci. China Earth Sci.* **2011**, *54*, 789–797. [CrossRef]
125. Goldfarb, R.J.; Santosh, M. The dilemma of the Jiaodong gold deposits: Are they unique? *Geosci. Front.* **2014**, *5*, 139–153. [CrossRef]